Journal of Volcanology and Geothermal Research 259 (2013) 145–169

Contents lists available at SciVerse ScienceDirect

Journal of Volcanology and Geothermal Research

journal homepage: www.elsevier.com/locate/jvolgeores

Character, mass, distribution, and origin of tephra-fall deposits from the 2009 eruption of Redoubt Volcano, Alaska—Highlighting the significance of particle aggregation

Kristi L. Wallace [a,*], Janet R. Schaefer [b], Michelle L. Coombs [a]

[a] Alaska Volcano Observatory, Volcano Science Center, U.S. Geological Survey, 4200 University Drive, Anchorage, AK 99508, United States
[b] Alaska Volcano Observatory, Alaska Division of Geological & Geophysical Surveys, Fairbanks, AK 99708, United States

ARTICLE INFO

Article history:
Received 26 May 2011
Accepted 22 September 2012
Available online 29 September 2012

Keywords:
Tephra
Isomass
Accretionary pellets
Redoubt
Volcanic ash
Aggregation
Aggregates
Fine ash

ABSTRACT

The 2009 eruption of Redoubt Volcano included 20 tephra-producing explosions between March 15, 2009 and April 4, 2009 (UTC). Next-Generation radar (NEXRAD) data show that plumes reached heights between 4.6 km and 19 km asl and were distributed downwind along nearly all azimuths of the volcano. Explosions lasted between <1 and 31 min based on the signal duration at a distal seismic station (86 km). From Moderate Resolution Imaging Spectroradiometer (MODIS) imagery and field data, we estimate that over 80,000 km^2 received at least minor ash fall (>0.8 mm thick), including communities along the Kenai Peninsula (80–100 km) and the city of Anchorage (170 km). Trace ash (<0.8 mm) was reported as far as Fairbanks, 550 km NNE of the volcano. We estimate the total mass of tephra-fall deposits at 54.6×10^9 kg with a total DRE volume of 20.6×10^6 m^3.

On March 15, a small (4.6 km asl) phreatic explosion containing minor, non-juvenile ash, erupted through the summit ice cap. The first five magmatic explosions (events 1–5) occurred within a 6-hour period on March 23. Plumes rose to heights between 5.5 km and 14.9 km asl during 2- to 20-minute-duration explosions, and were dispersed mainly along a NNE trajectory. Trace ash fall was reported as far as Fairbanks. Owing to a shift in wind direction and heavy snowfall during these events, field discrimination among many of these layers was possible. All deposits comprise a volumetrically significant amount of particle aggregates, yet only event 5 deposits contain coarse clasts including glacier ice. The most voluminous tephra fall was deposited on March 24 (event 6) from a 15 minute explosion that sent a plume to 18.3 km asl, and dispersed tephra to the WNW. Within 10 km of the vent, this deposit contains 1–11 cm pumice clasts in a matrix of 1–2 mm aggregate lapilli. A small dome was presumably emplaced between March 23 and March 26 and was subsequently destroyed during 1–14 minute magmatic explosions of events 7–8 (March 26) that sent plumes between 8.2 km and 19 km asl. Ash fell along a broad swath to the ESE, covering communities along the Kenai Peninsula with up to 1 mm of ash. Proximal deposits are largely composed of aggregate lapilli of 1–2 mm with very little coarse juvenile material. Events 9–18 (March 27) sent plumes between 5.2 km and 15.5 km asl during <1–11-minute-long explosions. Ash clouds dispersed along trajectories to the NE, ENE and N and event 17 deposited up to 1 mm of ash on upper Kenai Peninsula and Anchorage. A moderate-size dome was emplaced between March 29 and April 4 and was subsequently destroyed during event 19 on April 4 which lasted 31 min and sent ash to 15.2 km asl. The proximal deposit is principally composed of dense dome rock, unlike earlier events, indicating that event 19 was likely caused by dome failure. The cloud dispersed to the SE along a narrow trajectory and up to 1–2 mm of ash fell on the lower Kenai Peninsula.

Particle size data showing a preponderance of fine ash, even in the most proximal locations, along with the abundance of aggregate lapilli documented in most samples, confirms that particle aggregation played a significant role in the 2009 eruption and induced premature fallout of fine ash.

Published by Elsevier B.V.

1. Introduction

The 2009 eruption of Redoubt Volcano included 20 tephra-producing explosions; each lasting from <1 to 31 min, between March 15, 2009, and April 4, 2009 (Table 1; Fig. 1; Power et al., 2013). Plumes reached heights between 4.6 km and 19 km above sea level (asl) and were distributed downwind along nearly all azimuths of the volcano. Other eruptive products include at least three small lava domes, minor pyroclastic flows, and major lahars (Schaefer, 2012; Bull et al., 2013; Waythomas et al., 2013), somewhat similar to the volcano's last eruption in 1989–90. Owing to their wide dispersal by winds, particularly at flight levels, airborne ash plumes and ash fall are considered the second most significant hazards of this eruption next to lahar inundation (Schaefer, 2012; Waythomas et al., 2013). We estimate that over 80,000 km^2 received at least minor ash fall (0.8–2.0 mm), including communities along the

* Corresponding author. Tel.: +1 907 786 7109; fax: +1 907 786 7150.
E-mail address: kwallace@usgs.gov (K.L. Wallace).

0377-0273/$ – see front matter. Published by Elsevier B.V.
http://dx.doi.org/10.1016/j.jvolgeores.2012.09.015

Table 1
Summary of significant tephra-producing events of the 2009 eruption of Redoubt Volcano.

Event #[a]	Date	Time[b]	Duration (seismic-SPU)[c]	Maximum plume height[d]	Plume height source[e]	Plume direction[f]	Origin of plume[g]	Communities impacted
	Local AKDT	Local AKDT	(min)	(km)	Radar, PIREP, etc.	N, S, NE, etc.		Location, ash thickness
0	3/15/09	13:05	Undefined	4.6	PIREP	SE	Phreatic	None
1	3/22/09	22:34	2	5.5	FAA	NNE	Magmatic	None
2	3/22/09	23:02	7	13.4	FAA	NNE	Magmatic	Int. Alaska, <1 mm
3	3/23/09	0:14	20	14.6	USGS	NNE	Magmatic	Int. Alaska, <1 mm
4	3/23/09	1:38	38	13.1	FAA and USGS	NNE	Magmatic	Int. Alaska, <1 mm
5	3/23/09	4:30	20	14.9	FAA	NNW	Magmatic	Int. Alaska, <1 mm
6	3/23/09	19:40	15	18.3	FAA	WNW	Magmatic	None
7	3/26/09	8:34	<1	8.2	USGS	ESE	Magmatic	None
8	3/26/09	9:24	14	18.9	FAA and USGS	E	Magmatic	Kenai Pen., 1–2 mm
9	3/26/09	23:47	<1	12.5	USGS	E	Magmatic	None
10	3/27/09	0:28	7.0	14.9	FAA	ENE	Magmatic	None
11	3/27/09	8:39	8	15.5	FAA	N	Magmatic	None
12	3/27/09	17:34	2	14.6	USGS	NNE	Magmatic	None
13	3/27/09	19:24	4	15.2	FAA	N	Magmatic	None
14	3/27/09	23:19	2	14.6	USGS	N	Magmatic	None
15	3/28/09	1:19	4	14.6	USGS	N	Magmatic	None
16	3/28/09	13:40	6	5.2	FAA	N	Magmatic	None
17	3/28/09	15:29	6	12.5	USGS	ENE	Magmatic	N. Kenai Pen., ANC, Southcentral Alaska, 1–2 mm
18	3/28/09	19:23	11	14.6	USGS	NE	Magmatic	None
19	4/4/09	5:58	31	15.2	FAA	SE	Magmatic, dome collapse	Kenai Pen., 1–2 mm

Communities impacted: Kenai Pen., Kenai Peninsula; Int. Alaska, Interior Alaska as far as Fairbanks; and ANC, Anchorage.
[a] Event numbers are given for explosions for which an official notice was issued by the Alaska Volcano Observatory (AVO).
[b] Official onset times were derived from analysis of seismic station data.
[c] Duration of seismic signal at station SPU is used as a proxy for duration of plume generation.
[d] Plume heights from pilot reports are from the Federal Aviation Administration (FAA). Plume heights vary depending on the data source and only maximum plume heights are reported here. Maximum plume heights were determined from either FAA (Next Generation Radar (NEXRAD) or U.S. Geological Survey (USGS) Doppler radar (pointed at the vent) and have error of ±1.5 km (Schneider and Hoblitt, 2013).
[e] FAA, FAA-owned NEXRAD; USGS, USGS-owned Doppler radar; and PIREP, pilot report.
[f] Plume directions are based on satellite data, FAA NEXRAD, and eyewitness accounts.
[g] Origin of tephra plume (mechanism): phreatic, non-magmatic vent explosion; magmatic, ash plume originating from vent (deposit contains significant juvenile vesicular material); dome collapse (deposit is mainly dense dome material).

Kenai Peninsula (80–100 km) and the city of Anchorage (170 km; Fig. 1). Trace ash (<0.8 mm) was reported as far as Fairbanks, 550 km NNE of the volcano. Over the course of the eruption, hundreds of flights were canceled or rerouted and many communities along the path of these ash plumes were inconvenienced with minor ash falls on multiple occasions (Murray et al., 2009).

Winter-time eruptions at high-latitude volcanoes provide an unparalleled opportunity to document primary tephra fall deposits preserved in the snow pack. Previous eruptions of Redoubt have documented ephemeral tephra-ice aggregates (accretionary pellets) in tephra-fall deposits (Scott and McGimsey, 1994), which were also a dominant feature in this eruption. Particle aggregation is an important process because it is a critical parameter for consideration in ash dispersion and sedimentation models (Mastin et al., 2013), which is a growing field of research in ash-hazard analysis.

This report describes the timing, distribution, character, mass, and origin of tephra-fall deposits of the 2009 eruption of Redoubt Volcano and concludes with a discussion of their significance and hazards. Because most of the explosive events were not observed directly, we infer ash-plume characteristics from time-lapse photography, geophysical data, and deposit characteristics. Magmatic or hydro-magmatic explosions at the vent initiated most tephra falls, and dome collapse(s) or possibly a hybrid of both processes, initiated others. We include a section on tephra-ice aggregates to draw special attention to this process, to aid those developing ash dispersion and sedimentation models, and to gain insight in the interpretation of ancient deposits.

1.1. Geologic background and eruptive history

Redoubt Volcano is a 3108-m-high, ice-clad stratovolcano, located on the west side of Cook Inlet, within remote Lake Clark National Park, Alaska (Fig. 1). It sits 170 km southwest of Anchorage, and within 100 km of the Kenai Peninsula, together Alaska's most populous region. Prior to 2009, Redoubt had erupted three times historically, in 1902, 1966–68, and 1989–90 (Miller et al., 1998). These eruptions produced significant ash plumes above 12 km asl as a result of vent explosions and lava-dome collapses. The 1989–90 eruption caused significant disruption to air traffic including an aircraft encounter with an ash plume that caused engine failure and near disaster (Casadevall et al., 1994). Of the three previous historical eruptions, the 1989–90 eruption is the best documented and was most similar to the 2009 eruption in terms of erupted volume, products, and character, although fewer dome-collapse events occurred during the 2009 eruption (Brantley, 1990; Miller and Chouet, 1994; Scott and McGimsey, 1994). Abundant water supply at this ice-clad volcano contributes to processes such as particle aggregation in plumes and far-traveled floods and lahars (Dorava and Waythomas, 1995; Beget and Nye, 1994).

2. Methods

We describe tephra-fall deposits in terms of (1) time of eruption, (2) distribution, (3) character, including thickness, mass-per-unit area, particle size, composition (componentry), and preservation, (4) origin, and (5) significance. Appendix A includes three tables with detailed sample information including sample locations (Table A.1), raw particle size data (Table A.2), and samples used for component analysis (Table A.3). Samples collected for this study are archived at the U.S. Geological Survey (USGS) Alaska Tephra Laboratory and Data Center at the Alaska Volcano Observatory (AVO) in Anchorage, Alaska.

2.1. Timing and tephra production

We adopt the sequence and naming of eruption phases of Schaefer (2012) to describe the timing of the 2009 eruption. We use event numbers to reference individual explosions (Bull and Buurman, 2013; Schaefer, 2012; Table 1). We report explosion durations based on the signal

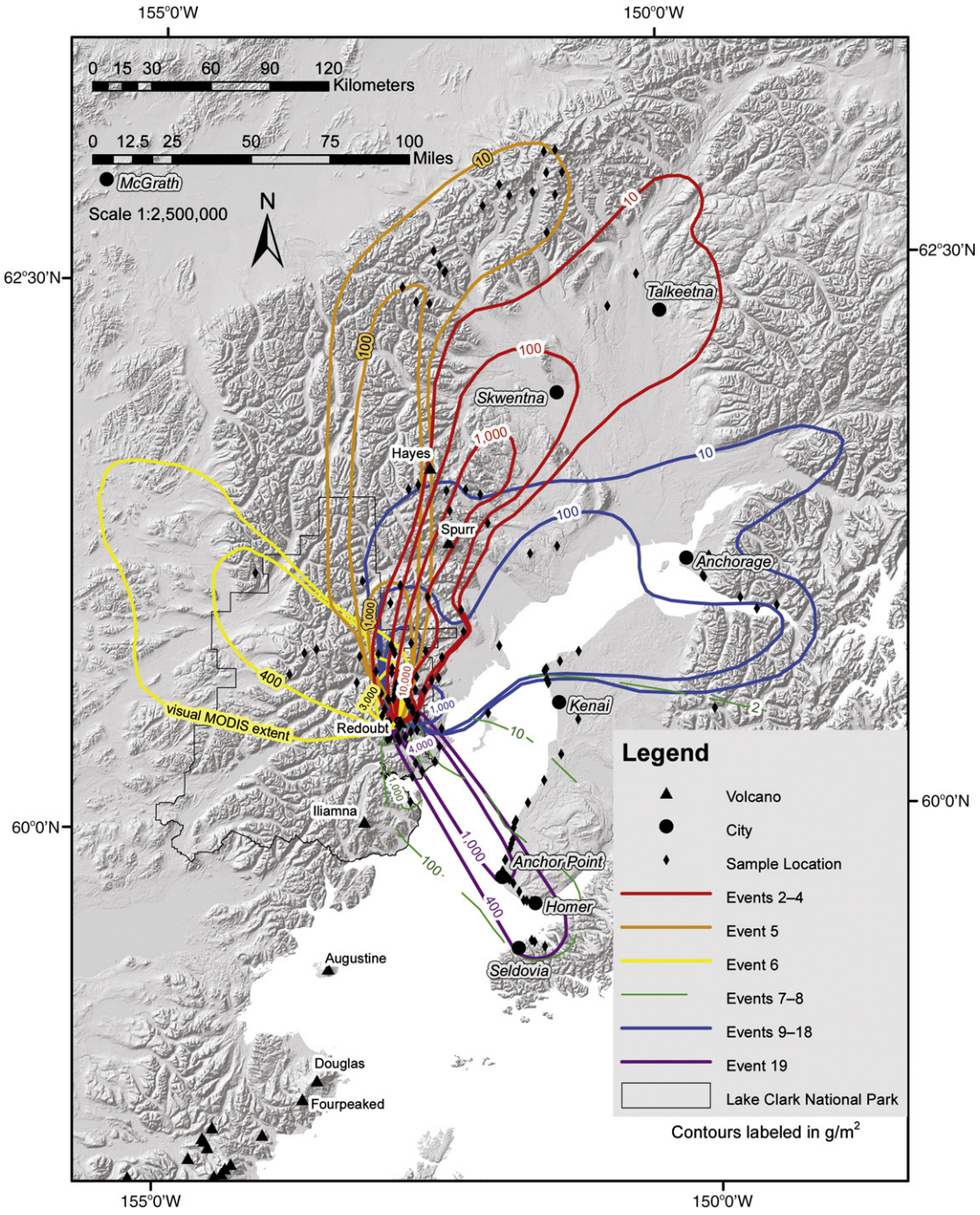

Fig. 1. Regional map of the Cook Inlet area, Alaska, showing the distribution of tephra-fall deposits of the 2009 eruption of Redoubt Volcano. Contours show isomass in g/m^2. Events refer to individual tephra-producing explosions that resulted in significant deposits (Table 1). Overlapping deposits that could not be separated in the field are reported as event packages (e.g., 7–8).

duration at a distal seismic station at Spurr Volcano, 86 km to the north (Power et al., 2013). Other sources of explosion durations are from more proximal geophysical stations near or on the flanks of the volcano. Plume heights are all derived from radar reflectivity data (Federal Aviation Administration (FAA) Next-Generation radar (NEXRAD) or U.S. Geological Survey (USGS) Doppler radar) except one that is from a pilot report (Table 1).

2.2. Tephra distribution

Explosions that generated discrete plumes had distinctive geophysical signals (Buurman et al., 2013; McNutt et al., 2013; Schneider and Hoblitt, 2013) that triggered the collection of plume data to guide tephra sampling. Data include: (1) estimation of plume height (from radar and/or pilot reports; Schaefer, 2012; Schneider and Hoblitt, 2013), (2) seismic and infrasound duration of explosive event (Buurman et al., 2013; McNutt et al., 2013), (3) direction of prevailing winds (National Weather Service), (4) direction of plume in satellite and radar data (Webley et al., 2013; Schneider and Hoblitt, 2013), (5) ash-fall reports from nearby towns and villages, and (6) overflight photography. Timely access to these data facilitated tracking of individual plumes and identifying areas for field sampling.

Reconstruction of plume trajectories from satellite images and radar reflectivity, at the time of plume generation and transport, closely

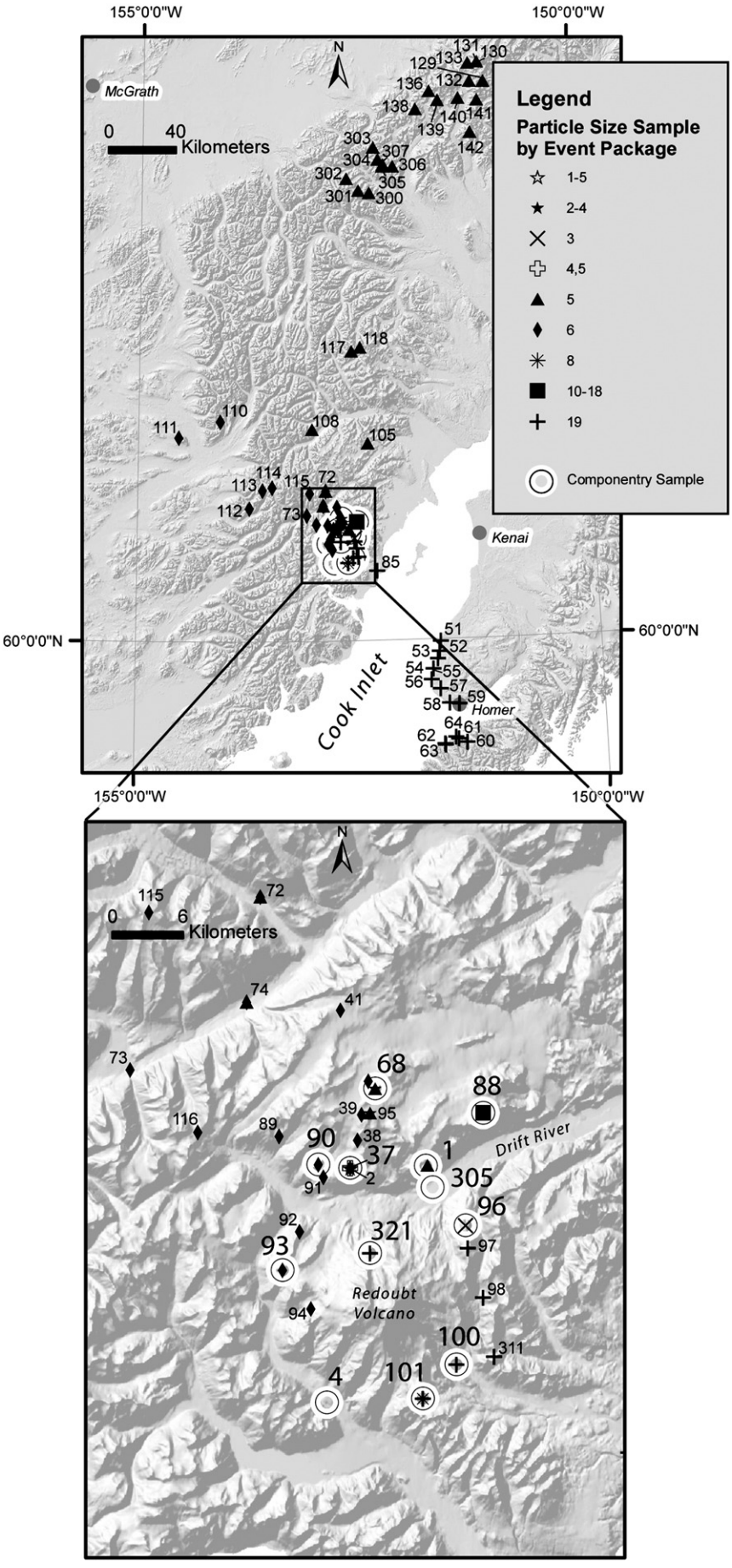
155°0'0"W
150°0'0"W
60°0'0"N
McGrath
0 40 Kilometers
Kenai
Cook Inlet
Homer
Legend
Particle Size Sample by Event Package
1-5
2-4
3
4,5
5
6
8
10-18
19
Componentry Sample
0 6 Kilometers
Drift River
Redoubt Volcano

match the wind forecast data from the National Weather Service (NWS) (Webley et al., 2013; Schneider and Hoblitt, 2013). Moderate Resolution Imaging Spectroradiometer (MODIS) satellite imagery was particularly valuable because it clearly showed tephra deposits on the clean white snow and through field sampling, we were able to roughly determine the minimum concentration of ash on the ground (with a white background) required to be seen in MODIS. Analysis of radar data at the time of plume generation and deposition facilitated the detailed mapping of tephra-fall deposits and allowed for strategic sampling. Two radar data sources were used: NEXRAD radar (operated by the FAA), Doppler radar (operated by the USGS). Radar technology obtains information based upon return energy and tends to resolve coarser particles compared to satellite imagery (Schneider and Hoblitt, 2013; Webley et al., 2013) thus proximal tephra-fall deposits were initially mapped using a Geospacial Information System (GIS) of radar data. Radar data are traditionally used to map weather (precipitation and wind) and so we also used these data to assess whether or not snow fall occurred at the time of deposition (along the path of a plume), which helped to interpret deposit stratigraphy at sampling sites. In many cases, tephra fall from multiple plumes occurred along the same trajectory within minutes to hours of one another, and so knowledge of intervening snow-fall layers (or lack thereof) helped to resolve deposit chronology at some sites.

Confirmation of tephra-fall deposits from initial maps derived from remote sensing data was done by helicopter, road-based field checks, or reports submitted by citizens. Due to the large uninhabited region affected by tephra fall and the great number of layers (20) within a two week time frame, our sample resolution is limited by (1) wide geographic range, (2) permitting constraints, and (3) the onset of spring thaw conditions which obliterated primary deposits.

2.3. Tephra collection and processing

We collected tephra-fall samples at 189 field stations between March 18 and July 11, 2009 (Figs. 1, 2 and Table A.1). For safety reasons, we were restricted from sampling closer than about 8–12 km of the vent, so near-vent samples are limited. We use the term proximal for the region within 15 km of the vent and distal as the region beyond. At each field station, we collected a bulk sample and a measured-area (0.04–0.16 m^2) sample of each deposit. At times, coarse-grained juvenile clasts were hand-picked from deposits for targeted analyses. Tephra deposits were preserved as a layer in or on the snowpack, which facilitated sampling of often thin and diffuse deposits. Several snow pits were excavated at each sample site to expose the deposit(s) and to select a representative sample. Snow overlying the tephra deposit was shoveled away, a plastic measured-area template was placed on top of the target deposit, and a trowel was used to trace out the measured area (Fig. 3). The tephra deposit and some underlying snow were collected by trowel into large plastic, sealable bags.

In the laboratory, measured-area samples were thawed at room temperature, gravity filtered to remove water, dried in a 60 °C oven, weighed, and mass-per-unit area was calculated by dividing the sample weight by the sample area.

In addition to the tephra collected by AVO staff, 139 samples (both measured-area and bulk samples) were voluntarily collected by citizens positioned within the depositional path of the plumes. The AVO website provides detailed instructions for making observations and collecting samples, which has been a very successful means for increasing our sample resolution and density (Wallace et al., 2010, and this report).

2.4. Tephra deposit characterization

We characterize tephra-fall deposits in terms of thicknesses, mass-per-unit area, grain size, composition (by component analysis), color, and particle aggregation.

We use standard volcanic terminology to characterize particle size (Fisher, 1961; Schmid, 1981; Chough and Sohn, 1990). Quantitative particle-size analyses of samples were completed by the USGS Cascades Volcano Observatory (CVO) Sediment Laboratory in Vancouver, Wash., using sieve and SediGraph techniques (Table A.2). Particle and deposit color is given using Munsell rock color notation. All particle-size data are of disaggregated samples and do not represent the size distribution of the primary aggregate-bearing deposits.

Component analysis was conducted on proximal coarse-grained (clasts >8 mm in diameter) deposits were sorted into categories based on macroscopic appearance including color and texture (Table A.3). Where coarse-grained material was not present in proximal deposits, we used the medium-ash to fine-lapilli fraction (particles 500 μm to 4 mm in diameter) and a binocular microscope to sort the various components of the tephra. We discovered that sorting clasts using a binocular microscope gave different results for some components compared to samples sorted by the naked eye. Some textures and colors appeared different under the brighter lighting conditions and greater magnification of the microscope, therefore, finer-grained samples were sorted into four generic categories and thus provide no direct comparison to coarse-grained samples (refer to Section 3.4 for results). Component densities were calculated using 30 clasts of each category from a single coarse-grained sample erupted during event 6 (Table A.1, 09RDKLW093). Clast densities were measured by a water immersion technique and converted to vesicularities using calculated dense-rock equivalent densities (Coombs et al., 2013) following methods of Houghton and Wilson (1989). Back-scattered electron images of thin sections of representative components were acquired using the USGS Scanning Electron Microscope in Anchorage, Alaska, and a 20-kV voltage.

Tephra aggregates were a dominant feature of all explosive phase tephra-fall deposits. We adopt the terms 'accretionary pellet' and 'ash cluster' from Brown et al. (2012) to describe ash aggregates documented in this eruption. The term accretionary pellet avoids particle size connotations associated with the more common term 'accretionary lapilli'. Most documented samples of accretionary pellets were described only qualitatively in the field before thawing. Select samples of accretionary pellets collected in March and early April when the temperatures remained below freezing were kept frozen for further analysis and photography.

2.5. Total mass erupted

We calculated total tephra-fall mass from 214 mass-per-unit-area measurements. Because most deposits fell mixed with snow or became mixed with snow after deposition, thickness measurements were not reliable. Collection areas ranged from 0.04 to 0.16 m^2 depending on the amount of ash present. Isomass contours (from 10 to 25,000 g/m^2) were constructed by hand for deposits of individual events or packages of undifferentiated events. MODIS imagery and FAA NEXRAD data guided contouring. Total mass of each tephra deposit was calculated using the root-area method developed by Pyle (1989) and modified by Fierstein and Nathenson (1992) (Table 2). This method accounts for the mass of tephra that fell beyond the most distal isomass contour. We calculate dense-rock equivalent (DRE) deposit volume by dividing the total mass by a rock density of 2650 kg/m^3 (averaged

Fig. 2. Regional map of the upper Cook Inlet area, Alaska, showing the locations of tephra-fall samples used for particle size and component analyses. Refer to Table A.2 for complete particle size data and precise locations. Inset shows the locations of proximal samples that were used for componentry. The prefix "09RDKLW" was omitted from sample locations for brevity. Refer to Table A.3 for a complete list of samples used for component analysis.

Fig. 3. Photograph showing an example of measured-area sampling guided by a 0.04 m^2 plastic template (red). Such samples yielded mass per unit volume measurements for contouring and calculation of total deposit mass (Fig. 1). Note the deposit thickness is ambiguous owing to compaction or melting of frozen aggregates pellets.

from calculated densities in Coombs et al., 2013) (Sarna-Wojcicki et al., 1981).

3. Results

In the following section, we describe in chronological order, the character of tephra-fall deposits of each tephra-producing explosion (Table 1) including distribution, field characteristics, aggregates, lithologic components, grain-size distribution (Table 2 and Table A.2), mass and volume, and preservation. We refer to deposits in the present tense even though most were not preserved as recognizable layers after the aggregates thawed and snow melted.

3.1. Distribution of tephra-fall deposits

The distribution of tephra-fall deposits is a function of a variety of parameters including meteoric influences such as wind direction, wind speed, and precipitation; and eruption parameters such as plume height, mass eruption rate, duration, particle density, particle-size distribution, and particle-aggregation processes (e.g., Mastin et al., 2009; Carey and Sparks, 1986).

Plumes generated during the 2009 eruption of Redoubt reached heights of 4.6 to 19 km asl with the majority over 12 km asl (Table 1). Explosion durations were relatively short, between less than 1 to 38 min but typically less than 10 min (Table 1; Power et al., 2013). Tephra plumes were distributed downwind along nearly all azimuths of the volcano. Reconstructions of tephra-fall deposits show that 15 of the 19 major tephra-producing plumes represent prevailing southwesterly winds (Fig. 1). Less common easterly and northwesterly winds distributed the remaining four plumes (events 6, 7, 8, and 19). We estimate that over 80,000 km^2 received at least minor ash fall (0.8–2.0 mm), including communities along the Kenai Peninsula (80–100 km; events 8, 17, and 19) and the city of Anchorage (170 km; event 17). Trace ash (<0.8 mm) was reported as far as Fairbanks, 550 km NNE of the volcano (events 2–5). Narrow plumes reflect strongly unidirectional wind patterns (e.g., event 19). Winter storm activity as tracked by NEXRAD radar was used to note where snow fall occurred during tephra-fall events and likely contributed to premature fallout of tephra. Tephra aggregation processes in all 19 plumes also contributed to premature fallout of tephra, particularly fine ash (refer to Sections 3.3 and 4.2). Tephra falls that were generated within a short time period (minutes to hours), distributed along the same trajectory, and not accompanied by snow fall, are treated as a composite layer and referred to as an "event package" identified by its event numbers. Only deposits from events 5, 6, and 19 could be discriminated as individual eruptive units (Fig. 1). Distal margins of tephra-fall deposits are not well known because they either were deposited in Cook Inlet or onto uninhabited regions beyond the reach of our field campaign. In addition to field observations, MODIS satellite imagery showed the visual extent of tephra deposits on snow. The limit of darkened snow likely represents an ash concentration of about 10 g/m^2 (Fig. 1). Other papers in this issue discuss airborne plume distribution as shown by other data sources such as satellite imagery and radar reflectivity (Schneider and Hoblitt, 2013; Steensen et al., 2013; Webley et al., 2013).

3.2. Field characteristics of deposits

All deposits are dark- to light-gray in color (Munsell color N7–N3, respectively) depending on whether they are wet or dry, respectively. Frozen primary deposits are typically medium to light-gray.

A phreatic explosion on March 15 deposited a small volume (covered an area of 3 km^2; 2 mm thick at 3 km from vent) of ash on the upper south flank of the volcano. Samples are fine grained (≤0.250 mm) and entirely composed of crystals and accidental lithic fragments; no evidence of juvenile material (vesicular particles or fresh-looking dense lithics) is present.

The first magmatic eruption began at 22:34 AKDT on March 22 and over the next 6 h, 5 distinct tephra plumes were generated (Table 1, events 1–5). The event 1 deposit was challenging to discern in the field except at one proximal location (Table A.1, 09RDKLW002) and is thought to be volumetrically insignificant based on short duration and low plume height and is not further discussed in this paper. Other than in locations where snowfall separated the deposits of events 2–4, deposits are generally not differentiated and are combined as an event package. Where differentiated, events 2–4 have similar deposit characteristics. Proximal deposits within 12 km of the vent are 1–4 cm thick poorly sorted clast-supported layers of frozen accretionary pellets in contact with fewer individual vesicular clasts (Fig. 4A).

A shift in wind direction toward the NW during the 3 h between events 4 and 5 allows better discrimination of the event 5 deposit, especially in distal locations (Fig. 1). The deposit 12 km from the vent is a few centimeters thick and contains the first evidence of coarse-grained (1–2 cm in diameter) vesicular clasts along with a volumetrically significant amount of frozen accretionary pellets (up to 8 mm in diameter) (Figs. 4 and 5A–E). Accidental subround ice clasts in the deposit, presumably fragmented from the summit crater glacier, are subequal in size to the largest vesicular clasts (Fig. 4). This unusual feature probably would not have been identified if not for visiting the site within a day of deposition, before burial or melting. Ice clasts were only documented at this location.

Fifteen hours later on March 23, event 6 produced one of the most significant plumes of the 2009 eruption (based on plume height, seismic duration, and deposit thickness). Southeasterly winds sent this plume to

Table 2
Summary of tephra-deposit characteristics for the 2009 eruption of Redoubt Volcano.

Event #[a]	Contours[b]	Max. prox. thick[c]	Max. prox. part. size[d]	Max. prox. agg. size[e]	Max prox. MPUA	Mass[f]	DRE volume[g]	Dense	Vesicular	Crystals	Lithics
	(g/m^2)	(cm)	(cm)	(mm)	(g/m^2)	($\times 10^9$ kg)	($\times 10^6$ m^3)	Component analysis[h]			
0	nd	0.3	nd	nd	nd	nd	nd	nd	nd	nd	nd
1–4	10, 100, 1000, 10,000	2	1.6	5	12,106	9.6	3.6	48.1	41.4	1.2	9.4
5	10, 100, 1000	3	8	10	6494	4.4	1.7	30.4	56.3	8.7	21.1
6	400, 3000, 20,000	5	11	5	23,970	15.1	5.7	25.0	66.5	0.0	8.5
7–8	100, 1000, 10,000	1.5	0.5	nd	2806	4.6	1.7	52.2	38.0	0.8	9.0
9–18	10, 100, 1000, 20,000	4	4	9	24,713	13.2	5.0	47.6	32.9	15.5	4.0
19	400, 1000, 4000, 25,000	5	1.6	nd	25,251	7.8	3.0	86.7	1.7	0.0	11.6
Totals						54.6	20.6				

Note: samples of events 7, 8, and 19 thawed before primary aggregates could be documented. Deposit thicknesses for events 7, 8, and 19 are therefore minimum values.
nd, no data.
[a] Event numbers are defined by explosions where a VAN/VONA was issued by AVO (Table 1).
[b] Contours used to construct isomass map for given event or package of events (see Sections 2.5 and 5).
[c] Maximum recorded proximal thickness is within 12 km of the vent. See Section 2.5 for a discussion cautioning the use of thickness data. Since we could not get closer than ~12 of the vent, these are not true proximal thickness.
[d] Maximum recorded proximal particle size is within 12 km of the vent.
[e] Maximum recorded proximal aggregate size is within 12 km of the vent. Aggregates refer to aggregate pellets common in the 2009 deposits.
[f] Mass calculations using root-area method (Pyle, 1989; modified by Fierstein and Nathenson, 1992) and based on plotting mass per unit area (MPUA) data on a base map and constructing isomass contours. The root-area method allows for extrapolation beyond the most distal isomass contour (Section 2.5).
[g] Dense Rock Equivalent (DRE) Volume based on a density of 2.650 g/m3 (average of calculated densities of 2009 lithologies (Coombs et al., 2013).
[h] Componentry, in wt.% of clasts in the ash to lapilli size fraction: Dense,dark-gray to light-gray low to high-silica andesite dense clasts; Vesicular, medium-gray to light-gray (rarely white) low to high-silica andesite scoria; Crystals, free crystals common in the sand size fraction; Lithics, nonjuvenile accidental clasts. Data are averaged for events with >1 sample, refer to Fig. 12 for detailed plots.

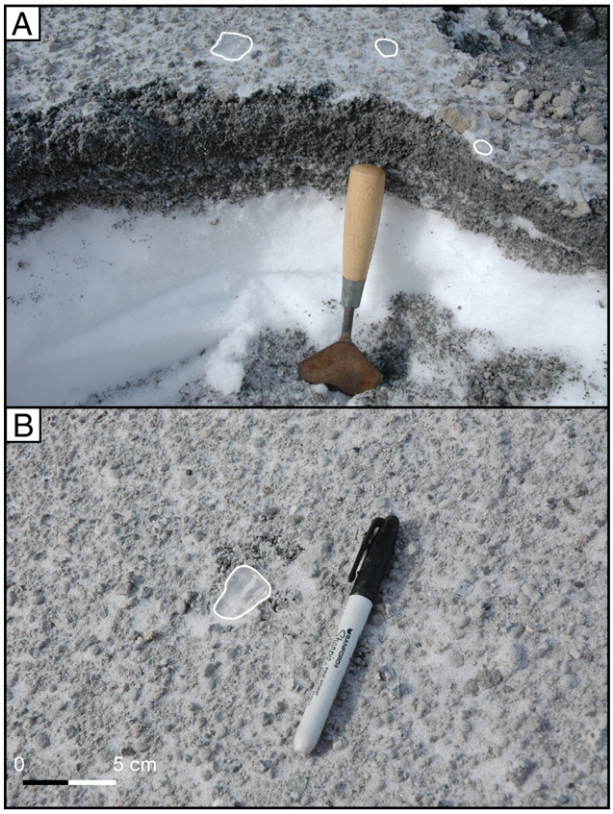

Fig. 4. Photograph of events 1–5 tephra-fall deposit at site 09RDKLW002 (Table A.1), 12 km from the vent. Note occurrence of accidental clasts of glacier ice which are found only in this deposit (outlined in white). Ice clasts are similar in size to the largest vesicular clasts (light- to medium-gray scoria) in this deposit. Section was photographed about 10 h after deposition. A) Cross-section of a composite tephra-fall layer of events 1–5 (Table 1); visible ice clasts are outlined in white and only found in the uppermost coarser-grained deposit (event 5); loose coarse vesicular clasts are shown in the right corner; trowel handle is 10 cm long. B) Surface of event 5 tephra deposit; single ice clast in this view is outlined in white and sits on the surface with abundant vesicular low-intermediate andesite clasts; black marker cap is 5 cm long.

the west of the volcano where no other 2009 tephra deposits exist (Fig. 1). Deposits within 10 km of the vent are 1–5 cm thick and contain the coarsest vesicular clasts of the eruption (up to 11 cm in diameter) as well as a volumetrically significant amount of clast-supported frozen accretionary pellets up to several millimeters in diameter (Figs. 6B and 7). Coarse clasts commonly burrowed into the snow surface leaving a cast that was subsequently backfilled with event-6 tephra (Fig. 6D).

On March 26, event 7 produced a small-volume tephra deposit restricted to the SE of the volcano (Fig. 1). Within an hour, event 8 occurred along the same trajectory albeit further traveled (longer duration) and thus its deposits are referred to as event package 7–8 in proximal locations. Event 8 resulted in 1–2 mm of fine-medium ash on communities of the Kenai Peninsula (Figs. 1 and 8B). No snowfall occurred for days after events 7 and 8 thus the deposits were exposed at the surface where dark-colored accretionary pellets thawed resulting in a continuous 1–2 cm mud layer in proximal locations (Fig. 8A) or a curd-like deposit in more distal locations where particles in the thin layer coalesced into clumps creating a discontinuous tephra layer (Figs. 6E and 8B).

Between March 26 and March 28, 10 tephra-producing explosive events and no snowfall resulted in a composite tephra layer (event package 9–18) to the NE, ENE and N of the volcano (Fig. 1). Snowfall on March 29 aided in insulating the composite layer and preserving primary frozen accretionary pellets although the surface of the layer (event 18) is often muddy, presumably from thawed pellets (Fig. 9A). The proximal deposit is a layer up to 3 cm thick (9 km from the vent) of clast-supported frozen accretionary pellets. Event 9, the lowest deposit, has accretionary pellets up to 9 mm in diameter that burrowed into the snow surface up to 4 cm deep (Fig. 9A). The event package 9–18 contains little disaggregated material coarser than a few millimeters in diameter. Of these 10 events directed towards population centers in south-central Alaska (Fig. 1), only event 17 on March 28 resulted in minor ($\leq$1 mm) fine- to medium ash fall on communities on the northern Kenai Peninsula and the city of Anchorage (Fig. 9B).

On April 4, the last tephra-producing explosion of the 2009 eruption sent an ash plume along a narrow trajectory to the SE of the volcano (Fig. 1). Prolonged exposure at the surface caused accretionary pellets to melt resulting in a mud layer up to 5 cm thick in proximal

locations (Fig. 8A). As in events 9–18, this deposit mostly lacked coarse clasts, even in proximal locations. Fine-medium ash fall, up to 2-mm thick, was deposited along the southern Kenai Peninsula (Fig. 8C).

3.3. Ash aggregates

Particle aggregation was a significant process in the 2009 eruption of Redoubt Volcano. Aggregates comprise a significant volume of the

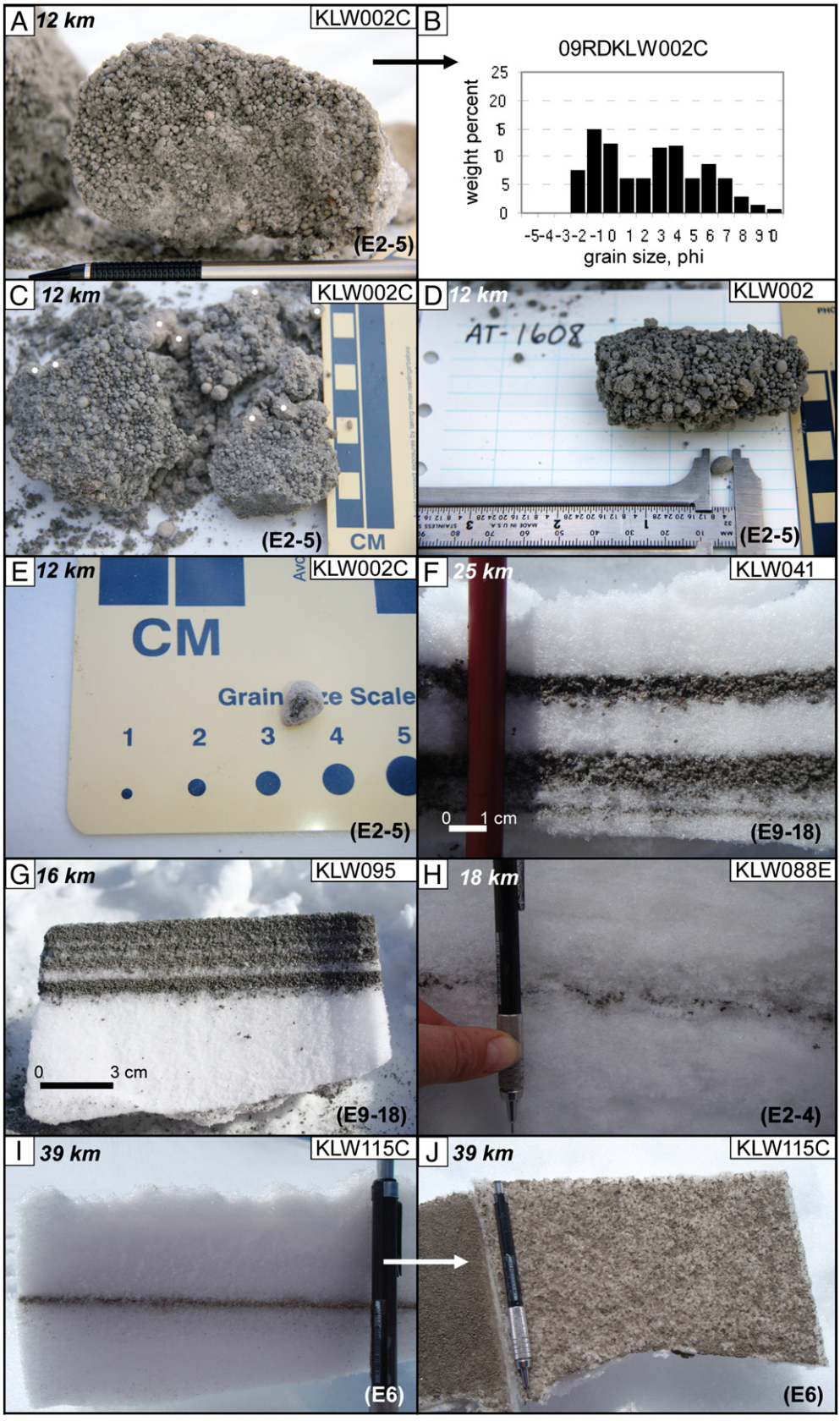

tephra, and are ubiquitous in all deposits regardless of origin (e.g., dome collapse, magmatic explosion), size of explosion (plume height, duration), or distance from source. Aggregates occur as both spherical 'accretionary pellets' comprised principally of fine ash and ice particles (most common, Fig. 5) and fragile, irregular-shaped 'ash clusters' comprised of fine ash that disaggregate on deposition (distal only). Accretionary pellets were ephemeral because they melted when exposed to above-freezing temperatures due to their significant ice content. With distance from source, aggregates appear to systematically become smaller in diameter and better sorted in deposits. For deposits that exist as mud layers or have a lumpy or curd-like texture, we infer that they originated as accretionary pellets or ash clusters (e.g., Fig. 6E–H, events 7–8, 19).

In proximal locations, accretionary pellets are larger (up to 9 mm) and more obvious, where they are round to sub-round, and form poorly sorted (1–10 mm in diameter) clast-supported layers comprised of both individual aggregates and individual pyroclasts (Fig. 5A–E). Spherical aggregates probably fell as frozen pellets because none are flattened by impact. Accretionary pellets in proximal deposits were frozen together and could not be easily separated, thus we have few measurements of individual aggregates. Table 2 shows maximum aggregate sizes in proximal locations by event or event package.

Both accretionary pellets and ash clusters were observed in distal locations. Accretionary pellets appear well-rounded, well-sorted, and smaller (up to 1 mm; Fig. 5F–I). They are preserved only in those deposits that were immediately covered by fresh snow after deposition. Unlike the ice-cemented deposits in proximal areas, the accretionary pellets in distal areas were not frozen together and appear as "dry" layers of spherical aggregates that melt quickly when exposed to the surface, forming a curd-like texture (Fig. 5I–J, respectively). Eye-witness accounts of ash clusters falling to the ground and disaggregating on impact were made by the senior author and other colleagues during ash fall in Anchorage (170 km) and Nikiski (80 km) on March 28 (event 17).

To assess the composition and character of individual aggregates, we hand-picked individual lapilli-size accretionary pellets from a proximal sample (09RDKLW002, Table A.1), measured them and allowed them to melt in the laboratory. Of the 80 sampled lapilli, all were composed of fine ash and only a few had coarse particle cores (Fig. 5E). None had obvious concentric rings or bands although high-resolution imaging was not performed. Individual lapilli were not large enough for grain-size analysis so, to assess the particle-size distribution of ash comprising individual accretionary pellets, we analyzed a single bulk section of a proximal deposit containing a volumetrically significant fraction of aggregate lapilli (Fig. 5A). Fig. 5B shows the particle size distribution of this poorly sorted deposit where the coarsest fraction (lapilli, −1 to −2ϕ) is of individual clasts and the fine fraction (ash, 0 to 10ϕ) is of disaggregated accretionary pellets.

3.4. Lithologic components

Tephra-fall deposits are the best stratigraphically constrained deposits of the eruption and thus they were used for component analysis to document the diversity of pyroclasts to assess changes in composition and eruptive process (e.g., degassing, eruptive style, magma ascent, fragmentation) throughout the eruption (this paper and Coombs et al., 2013). Clasts sorted into categories based on color and texture, yielded 7 principal components all associated with the explosive phase of the eruption (Fig. 10). Compositions shown here are from Coombs et al. (2013) and vesicular material is referred to as "scoria" throughout although varying degrees of vesicularity are exhibited (Table 3, Fig. 11).

(1) Medium-gray scoria (Munsell 5Y 6/1; low-silica andesite; Fig. 10A). Clasts are varying shades of brownish-gray-green; larger ones have highly inflated interiors and are variably oxidized. Makes up 45–50 wt.% of sampled fall deposits.
(2) Light-gray scoria (Munsell 5GY 8/1; intermediate to high-silica andesite; Fig. 10B). Light gray (rarely white), salt-and-pepper scoria clasts, composes 10–20 wt.% of all sampled fall deposits. Rubbly exteriors. Moderately to highly vesicular, some with vague banding from white to light gray.
(3) Dark-gray dense clasts (Munsell N3; unanalyzed; Fig. 10C). Dense, glassy, angular clasts, interpreted to be juvenile. Makes up to 2–8 wt.% of fall deposits.
(4) Medium-gray dense clasts (Munsell N5; unanalyzed; Fig. 10D). Dense with minor vesicles, angular, interpreted to be juvenile. Makes up 7–69 wt.% of fall deposits.
(5) Light-gray dense clasts (Munsell N6; unanalyzed; Fig. 10E). Dense with minor vesicles, angular, interpreted to be juvenile. Makes up 7–19 wt.% of fall deposits.
(6) Color-banded scoria clasts (unanalyzed; Fig. 10F). Variably vesicular with sharp to diffuse banding between light and dark gray, these compose <5 wt.% of clasts in measured samples.
(7) Non-juvenile lithics (unanalyzed; Fig. 10G). Altered and/or oxidized, relatively dense clasts that appear to be accidental lithics and make up 8–16 wt.% of fall deposits.

Pyroclast densities are used to characterize textural variations among erupted products. Average densities range from 700 kg/m^3 for the vesicular clasts to 2750 kg/m^3 for dense clasts and vary considerably within individual lithologies (Table 3). Microtextures of representative principal components (excluding accidental lithics) are shown as Scanning Electron Microscope (SEM) images (Fig. 11). Using the vesicularity classes of Houghton and Wilson (1989, Table 2), the dense pyroclasts are none to incipiently vesicular (0–19 vol.%), light-gray and medium-gray scoria clasts are high to moderately vesicular (perhaps more pumiceous than scoriaceous) and banded clasts are poor to moderately vesicular (35–53 vol.%).

Because we could not get closer than about 8–12 km from the vent for safety reasons, some of our most proximal samples either do not contain coarse material (lapilli) or, at this distance, coarse material is absent (i.e. fell as aggregates of fine material). As a result we only have coarse pyroclasts from events 2–6 and 19. All other sampled events are fine lapilli and smaller (≤4 mm). Therefore, as discussed in Section 2.4, finer-grained samples are sorted into four general categories, (1) "dense", (2) "vesicular", (3) "crystals", and (4) non-juvenile "lithics" and thus provide no direct comparison to coarse-grained samples. Finer-grained samples may be skewed toward the dense classification because as the sizes of the clasts converge with the diameters of the vesicles in them, the density increases and crystals get liberated (Walker, 1981) so even if their coarse counterpart was vesicular, we may have sorted them as dense. In this paper we combine all individual lithologic components (fine and coarse samples) into these 4 basic categories and use the data to interpret the origin of individual explosions (refer to Section 4.1). Refer to Coombs et al. (2013) where whole-rock

Fig. 5. Deposits of aggregate pellets formed during the 2009 eruption of Redoubt Volcano. Sample names, excluding the prefix "09RD" (omitted for brevity), distance from source, and event number (Table 1) of each deposit are labeled. Refer to Table A.1 for detailed sample information. Aggregates melt quickly when exposed to solar radiation and thus are not preserved in the geologic record. A) Intact frozen block of aggregate pellets; black mechanical pencil grip to tip length is 5 cm. B) Particle-size distribution for the section shown in A. C) Poorly-sorted proximal block of aggregate pellets showing co-existence with coarse scoria clasts (with white dots). D) Individual 6 mm aggregate pellet plucked from frozen block, shown above in photograph. E) Individual aggregate pellet with coarse lithic core. F) Well-sorted aggregate pellets preserved between snow layers; individual aggregates about 1 mm in diameter. G) In-situ primary aggregate pellet deposit; individual aggregates vary in size between events (layers). H) Discontinuous 1-mm layer of 1-mm diameter ice-tephra aggregates preserved in snow; pencil grip is 3 cm. I) 2-mm-thick distal primary aggregate pellet layer preserved in snow. J) Muddy curd-like result of exposing the surface of the primary aggregate pellet layer (shown in I) to solar radiation.

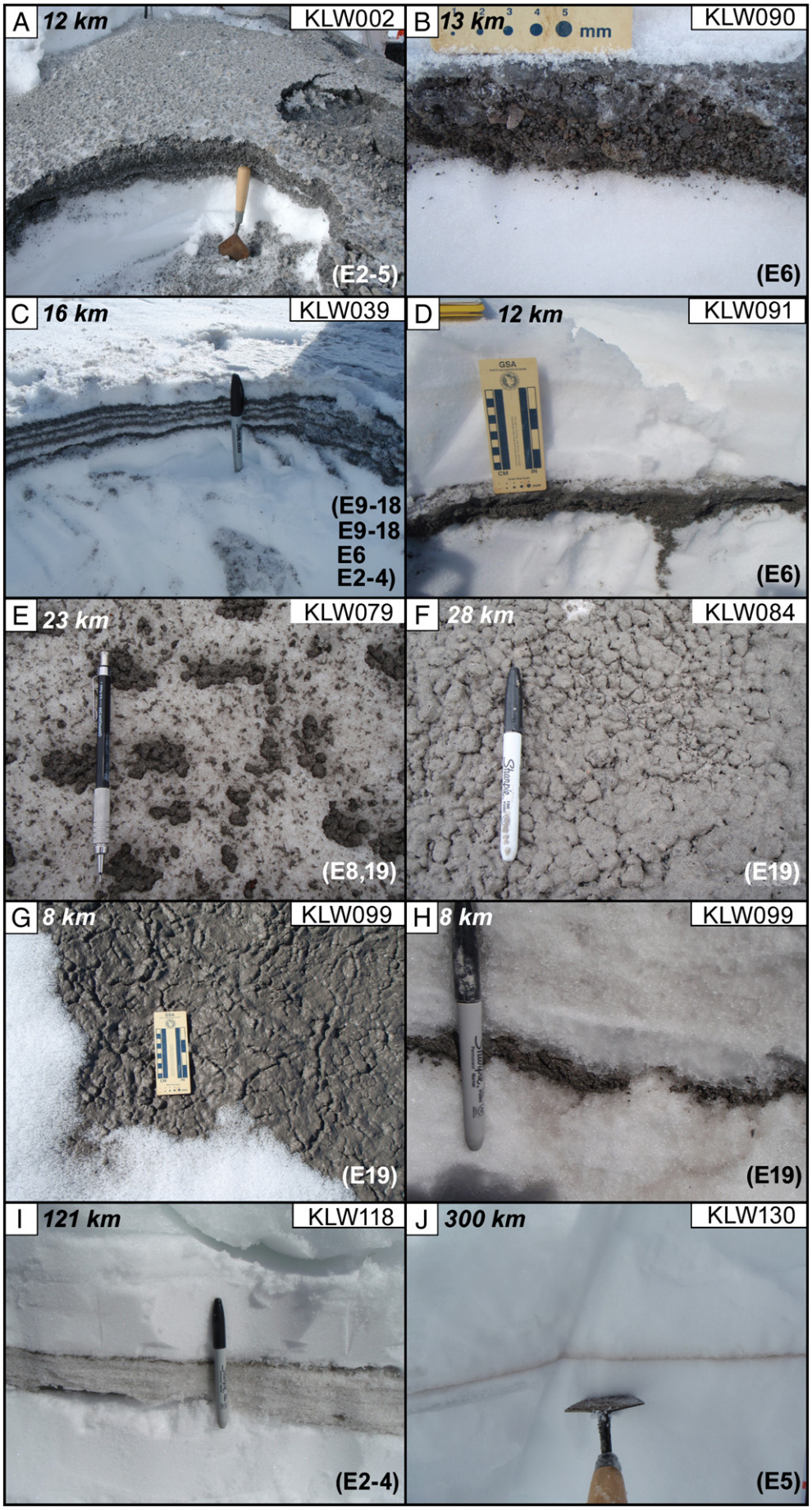
A
12 km
KLW002
(E2-5)
B
13 km
KLW090
(E6)
C
16 km
KLW039
(E9-18
E9-18
E6
E2-4)
D
12 km
KLW091
(E6)
E
23 km
KLW079
(E8,19)
F
28 km
KLW084
(E19)
G
8 km
KLW099
(E19)
H
8 km
KLW099
(E19)
I
121 km
KLW118
(E2-4)
J
300 km
KLW130
(E5)

Fig. 7. Photograph of large (11 cm maximum) vesicular low-silica andesite clasts erupted during event 6 on March 23, 2009. Clasts are variably oxidized and interiors are often more inflated than exteriors.

compositions of the principal lithologies are used to discuss variations in composition throughout the eruption.

Fig. 12 shows the distribution of the dense and vesicular material, crystals, and lithics in deposits from all events. Each column represents one sample. We did not include event 0 erupted on March 15 in our analysis because the deposit did not contain juvenile material. The following is a summary of the component data in chronologic order for each event or event package. Discussion of these data is in Section 4.1.

(1) Events 2–4 (March 22–23) samples are all fine-grained and contain the first evidence of vesicular material (22–54 wt.%) as well as a significant fraction of dense clasts (38–72 wt.%).
(2) Event 5 (March 23) samples contains both coarse and fine material dominated by vesicular clasts (55–57 wt.%), followed by dense clasts (28–32 wt.%) and accidental lithic clasts (12–30 wt.%).
(3) Event 6 (March 26) samples are all coarse-grained and dominated by (66–67 wt.%) vesicular material.
(4) Events 7–8 (March 26) samples are all fine-grained and contain roughly subequal amounts of vesicular and dense material. The high proportion of dense material (49–55 wt.%) may reflect differences in sorting fine material as discussed earlier in this section.
(5) Events 9–18 (March 27–28) samples are all fine-grained and have subequal amounts of vesicular and dense material. A single sample of events 9–18 (Table A.3, 09RDKLW096B) collected 10 km from the vent has significantly more dense clasts compared to other samples of the same package. The sample is very small and is more proximal than the other samples which may account for the greater proportion of dense material. The abundant free crystal fraction (12–18 wt.%) in events 9–18 samples is because the grain size of the sample is equal to the size of liberated crystals (mostly plagioclase crystals but also minor amounts of amphibole and pyroxene). Events 9–18 are the finest-grained samples of the 2009 eruption (see Section 3.5).
(6) Event 19 (April 4) samples are dominated by dense clasts (82–90 wt.%), mainly medium-gray high-silica andesite (Fig. 2C of Coombs et al., 2013). Clasts are of the same composition as dome lavas that extruded between April 4 and July 1, immediately after event 19.

3.5. Grain-size characteristics of selected deposits

Of the 20 tephra-fall deposits of the 2009 eruption, we performed quantitative particle-size analyses on samples from events 5, 6, and 19, because they were the only deposits that we could discriminate as individual layers in the field. All other deposits are composite layers of multiple events. Particle size analyses of such composite layers were completed for a few samples collected within 18 km of the vent to aid in component analysis (Fig. 2 and Table A.2).

Particle size distributions at various distances from the vent are used to characterize tephra fall deposits. Grain-size data for events 5, 6, and 19 are summarized on plots of weight percent versus grain size in phi (ϕ) units (Fig. 13). Fig. 14 shows weight percent of fine ash ($\geq 4\phi$; ≤ 63 μm) with distance from the vent (Table A.2). Data for one sample from event 8 and 6 samples from composite layers for events 1–5 and 9–18 are given in Table A.2, but not plotted in Fig. 13. Observations from these data include:

(1) Event 6 contains the coarsest material of the 2009 eruption followed by event 5, events 2–4, 8, 19 and finally 9–18.
(2) Event package 9–18 fall deposits are among the finest-grained samples of the eruption and contain almost no lapilli-size fraction (09RDKLW088A, Table A.2). We sieved several other samples to verify this observation and could find only rare material coarser than about 3–4 mm in diameter.
(3) Event 19 fall deposit is composed almost entirely of ash-size particles ($\geq 0\phi$). Sample 09RDKFB321A, 4 km from the vent is from a pyroclastic flow and is the only sample with a significant lapilli fraction ($\leq -1\phi$) (Fig. 13C).
(4) Ash-size particles (0 to 10ϕ) dominate even in proximal samples.
(5) A significant fine-ash ($\geq 4\phi$; ≤ 63 μm) fraction is observed in all samples, regardless of distance from source. Up to 67 wt.% fine ash within 20 km of the vent for events 5, 6, and 19.
(6) The fraction of fine ash with distance from the vent is highly irregular and non-systematic.

Fig. 6. Variations in tephra-fall deposit characteristics on snow. Sample names, excluding the prefix "09RD" (omitted for brevity), distance from source, and event number (Table 1) of each deposit are shown on each photograph. Refer to Table A.1 for detailed sample information. A) Five primary tephra deposits with little intervening snow fall; handle of trowel is 10 cm. B) Primary sequence of aggregate pellets and coarse scoria clasts on fresh snow. The upper 1 cm is a frozen mass of melted aggregate pellets caused by exposure to solar radiation while at the surface before snow fall occurred. C) Sequence of 5 tephra-fall layers that were easily discriminated due to intervening snow falls; black cap on marker is 5 cm. D) Coarse clasts deposited during event 6 burrow into the low density snow surface upon impact and are backfilled by aggregate pellets during the tephra-fall event; scale shows cm on the left and inches on the right. E) Curd-like texture of tephra-fall deposit that was exposed to solar radiation causing the aggregate pellets to melt and coalesce. This deposit originated as a continuous thin layer of aggregate pellets on snow. F) Lumpy texture of melted aggregate pellets. This deposit originated as a continuous thick layer of aggregate pellets on snow; black cap on marker is 5 cm. G) Slurry of melted aggregate pellets; this deposit was so watery that it was actually flowing on the surface; scale shows cm on the left and inches on the right. H) Muddy tephra layer of melted aggregate pellets; melting in this case occurred in place before exposure to the surface due to warm April outside temperatures. I) Distal composite tephra-fall layer that occurred during a snow fall event; black cap on marker is 5 cm. J) Distal primary tephra layer buried deep in the snow pack where aggregate pellets are not melted.

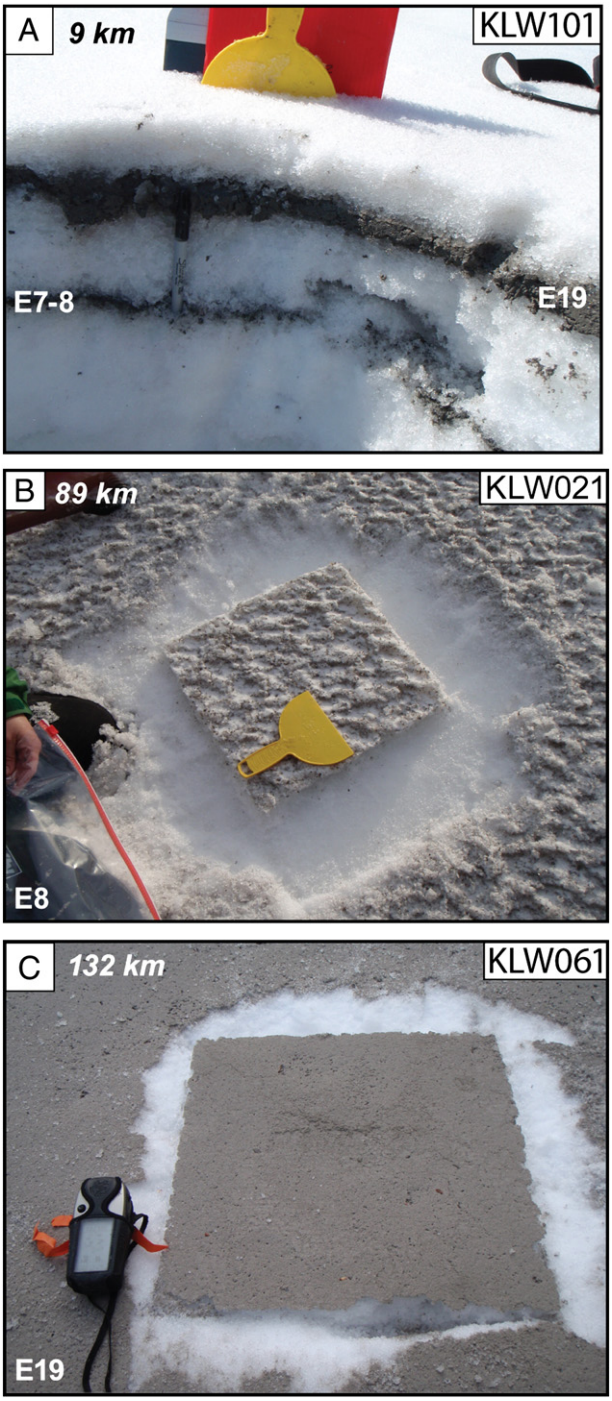

Fig. 8. Photographs of tephra-fall deposits of events 7, 8, and 19 (Table 1) at various distances southeast of Redoubt. Station name, excluding the prefix "09RD" (omitted for brevity), distance from source, and event number (Table 1) of each deposit are shown on each photograph. Refer to Table A.1 for detailed sample information. A) Muddy melted aggregate pellet layers preserved in the snow pack; event 19 deposit is 1–2 cm thick (up to 5 cm thick, not shown in this photograph); thicker than the 1–1.5 cm composite layer comprising events 7 and 8. B) Measured area (0.16 m^2) of event 8 tephra-fall deposit near Anchor Point, Alaska. Deposit is 1 mm thick and has a curd-like, lumpy texture because the deposit is dark-colored and absorbed solar radiation accelerating the rate of snow and ice-tephra aggregate melting. C) Measured area (0.16 m^2) of event 19 tephra-fall deposit in Seldovia, Alaska. Deposit is 2 mm thick and unmodified by melting because it was sampled only a few hours after deposition on a cold day.

Fig. 9. Photographs of tephra-fall deposits of explosive events 9–18 (Table 1) at various distances northeast of Redoubt. Sample name, excluding the prefix "09RD" (omitted for brevity), distance from source, and event number (Table 1) of each deposit are shown. A) Proximal composite tephra fall-deposit of explosive events 9–18; events could not be differentiated in the field because they occurred over a short time period with no intervening snow fall. Visible at the base of the deposit are 4–5 mm aggregates that penetrated into the low-density snow surface upon impact; scale shows cm to the left and inches on the right. Inset shows that aggregate pellets dominate this deposit; marker is 7 cm. B) Distal 1-mm thick tephra-fall deposit of explosive event 17 in Anchorage, Alaska. Of the 19 tephra plumes of the 2009 eruption, only event 17 (March 28) resulted in ash fall on Alaska's most populous city.

(7) Mean grain size generally decreases with distance from vent but there is a distinct fine fraction at all locations, i.e., the coarse mode diminishes with distance but the finer mode persists with distance from source.

(8) All samples are poorly sorted although sorting improves with distance.

(9) Most data are fine-skewed.

(10) Coarse particles from site KLW130A, B (Fig. 13A), 300 km from the vent are probably wind-blown material from the nearby bedrock exposure. The data otherwise are comparable with sample KLW131B near the same location. This location at the 14,200-ft base camp on Mt. McKinley is notoriously windy.

3.6. Mass and volume of tephra-fall deposits

The mass of tephra-fall deposits is used as a measure of the magnitude of individual events (Table 2) as well as in the determination of the mass and volume of magma that was erupted explosively and transported as ash clouds. Combined with other products of the eruption (pyroclastic flows, lava flows, domes, lahars) total eruption mass can be determined (Bull and Buurman, 2013). Our ash fall isomass and sample location map is available as digital vector shape files (Schaefer and Wallace, 2012).

Based on mass-per-unit area (MPUA) data from 214 samples, we estimate the total mass of tephra-fall deposits for the 2009 eruption of Redoubt Volcano at 54.6×10^9 kg with total DRE volume of 20.6×10^6 m^3. The mass of tephra fall for individual explosive events could only be estimated for events 5, 6, and 19 and ranges from 4.4 to 15.1×10^9 kg, similar to those of the 1989–90 eruption of Redoubt (Scott and McGimsey, 1994, Table 1). The event 6 deposit (March 23) has the largest estimated mass of the eruption (15.1×10^9 kg), even when compared to the mass estimates for combined deposits (Table 2) which is consistent with our field observations of maximum deposit thickness, particle size, plume height, and eruption duration (Table 1). The DRE volume of the event 19 (April 4) tephra-fall deposit (3.0×10^6 m^3) is smaller than the estimated volume of the dome that collapsed on April 4 (Bull and Buurman, 2013; Diefenbach et al., 2013), which is consistent with some of the dome volume contributing to the small pyroclastic flow and lahar generated during this event (Schaefer, 2012).

Uncertainties in tephra-fall mass estimates can be attributed to inaccuracies in construction of isomass contours and uncertainties in the method of calculation. The accuracy of reconstructions varies among events and event packages and is based on the number and position of samples with respect to the distribution of the deposit. Irregularity of MPUA values, especially in proximal areas may be due to (1) pulses in ash clouds from syn-eruptive injections of ash from pyroclastic flows and surges, (2) uneven tephra distribution caused by topographic controls on the movement of ash clouds, (3) irregular rates of particle aggregation in the ash cloud, and (4) wind reworking of deposits. Because most deposits were either immediately buried by snow or fell as frozen accretionary pellets that formed ice-cemented deposits, we do not attribute irregularities in MPUA values in proximal areas to wind reworking. Uncertainties in the mass estimates using the root-area method (see Section 2.5) are reflected in the fitting of the mass data to a straight line (single slope line) or two linear segments (two-slope line). Fig. 15 shows plots of MPUA versus the square root of isomass area for all fall deposits. Data are best fitted to two-slope line for all estimates except event 5 which are best fitted to a single-slope line.

3.7. Preservation of tephra deposits

Preservation of tephra-fall deposits is an important consideration for the future interpretation of these deposits and prehistoric tephra-fall records from this volcano and others in this region. Preservation of tephra-fall deposit characteristics (including aggregates and discrete layers) from the 2009 eruption is compromised mostly by spring thaw conditions and the preponderance of fine ash in deposits. Tephra-fall on snow, although very convenient for sampling and discriminating deposits, ultimately contributes to the poor preservation of original fall deposit characteristics. Above-freezing temperatures cause both the snow to melt and the frozen accretionary pellets to thaw to mud, obliterating these deposit characteristics in the final deposit. By May 2009, most tephra-fall layers coalesced into a single composite layer on the landscape and lack any evidence of having originated as multiple deposits or as layers comprised dominantly of aggregates. This also may suggest that deposits documented along prevailing wind directions are likely to be thicker (as they are in this study) as a result of coalescing of originally discrete layers. This is particularly important to consider in tephrostratigraphic studies where deposit thickness may be used to characterize the size of an eruption. Distal event 5 and 6 deposits, northeast and west of the volcano, are the only deposits of the 2009 eruption that do not overlap with other tephra-fall deposits and therefore will potentially be preserved as discrete layers. The high proportion of fine ash in all deposits is susceptible to reworking by surface processes. Reworking of fine ash for days to months after the eruption was a commonly reported. All 2009 fall deposits, if preserved, will retain their poorly sorted character resulting from premature fallout of fine ash due to particle aggregation in the plume.

4. Discussion

4.1. Origin of tephra-fall deposits

Multiple volcanic processes can generate ash clouds and ash fall—short-lived blasts, either magmatic or phreatic (or both); sustained magmatic eruption; and elutriation of ash from pyroclastic flows. Integration of field observations and laboratory analyses of tephra-fall and other deposits of the 2009 eruption of Redoubt Volcano is critical to interpreting the origins of the fall deposits. Close coordination with researchers who studied other aspects of the eruption (e.g., Bull and Buurman, 2013; Coombs et al., 2013; Buurman et al., 2013; Waythomas et al., 2013) allowed for consistent identification and characterization of all eruptive products. Evidence used to interpret deposit origin includes: (1) duration of plume generation and plume height, (2) volume of fall deposits, (3) componentry of fragmental deposits, (4) grain-size data, (5) contemporaneous volcanic activity, (6) seismicity, (7) infrasound pressure-sensor signals, and (8) gas and steam emissions. The following discussion is focused on the origin of tephra-fall deposits in chronological order throughout the 2009 eruption. Discussion of the origin of the fine-grained character of the tephra-fall deposits and associated aggregates is presented in Section 4.2.

The small explosion on March 15 (event 0, Table 1) resulted in a small-volume tephra deposit that does not contain juvenile material and is considered a pre-magmatic, phreatic explosion. This is consistent with the fine-grained hydrovolcanic character (efficient magma–water fragmentation) of the deposit and with gas analyses from overflights on March 15 and 20 which suggest that magma was still at depth beneath the surface (Werner et al., 2013).

Explosions of March 22–23 (events 1–6, Table 1) are interpreted to result from magmatically-driven explosions. Events 1–6 were preceded by a long-duration seismic swarm beginning on March 20, part of which is interpreted as dome growth (Buurman et al., 2013). Satellite data show that a very small dome (115×75 m) was emplaced during a 10-hour period on March 22, prior to the first explosion (Schaefer, 2012; Bull and Buurman, 2013, Diefenbach et al., 2013). Component data (see Section 3.4, Fig. 12) show that the first juvenile material of the eruption was erupted on March 22–23. Deposits from events 1–6 contain 25–48 wt.% dense juvenile material with proportionally more in the early events (2–4, Fig. 12), presumably contributed by destruction of the small dome extruded prior to explosive activity. Dense lithic fragments documented in lahar deposits generated during this time (Waythomas et al., 2013) may be fragments of the small dome. The proportion of vesicular material increases toward events 5 and 6 (56–66 wt.%, respectively) that produced the coarsest material of the eruption (Figs. 12B and 7). Accidental lithic clasts make up a significant amount of event 5 samples (12–30 wt.%) and probably result from incorporation of wall rock during vent widening. Accidental ice clasts documented in the event 5 deposit are presumed to be fragments of the Drift glacier that occupied the vent area prior to these explosions. Seismic data between events 5 and 6 on March 23 show high-amplitude tremor consistent with magma movement toward the surface (Buurman et al., 2013). The first pyroclastic flow of the eruption occurred during event 6 which is consistent with seismic data and the elutriation of fine ash from the flow may account, in part, for the fine-grained nature of aggregates in the deposit. Because the dome of March 22 was very small, dome collapse is unlikely to have initiated these events, rather; dome emplacement likely played a role in pressurizing the shallow magmatic system leading to explosive eruption.

Explosions of March 26 (events 7–8, Table 1) are interpreted to result from magmatically-driven explosions that destroyed an existing

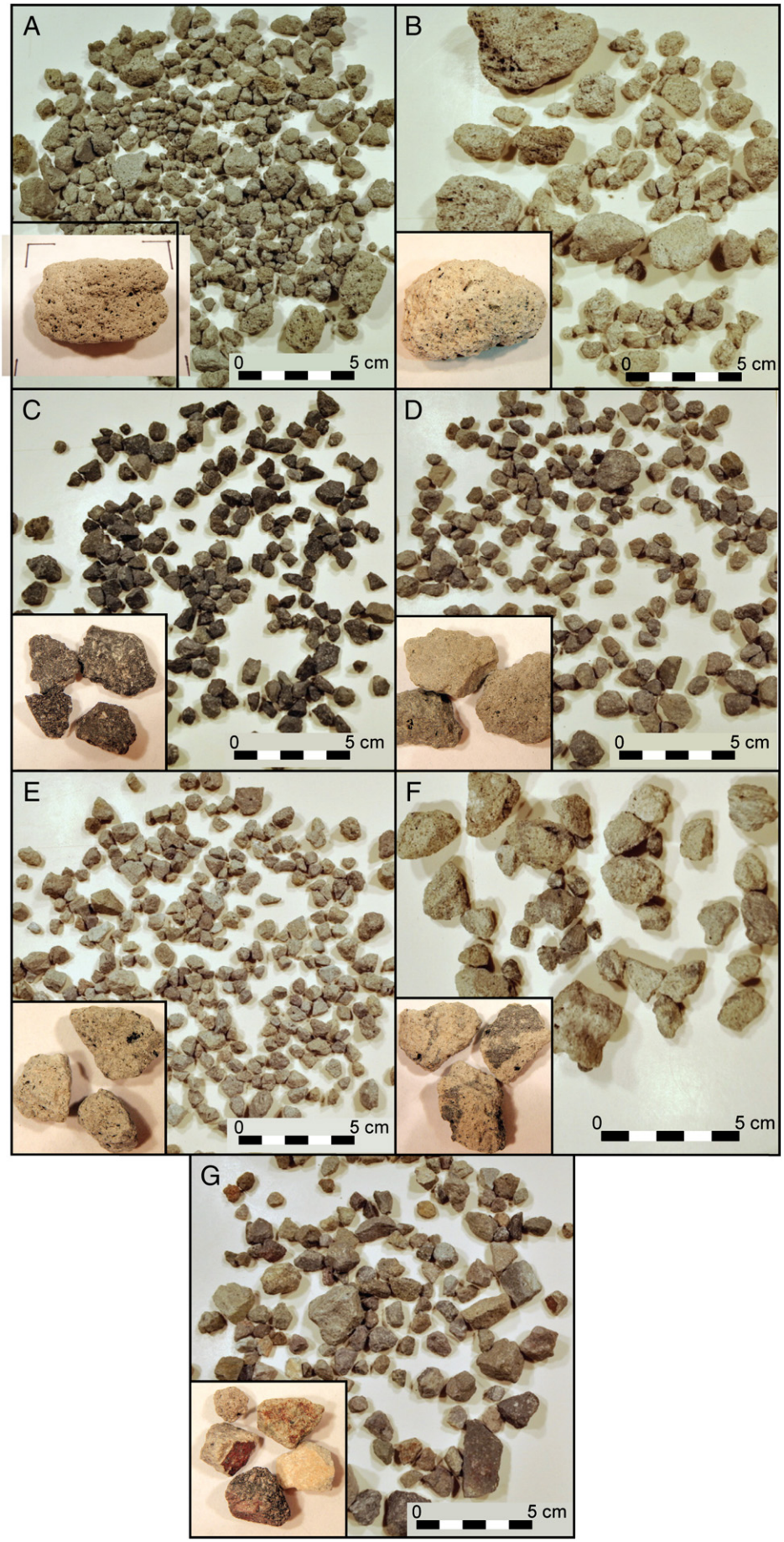
A
0
5 cm
B
0
5 cm
C
0
5 cm
D
0
5 cm
E
0
5 cm
F
0
5 cm
G
0
5 cm

Table 3
Summary of 2009 pyroclast densities of major juvenile components from sample AT-1823 of event 6.

Component lithology	Median (kg/m^3)	Mean (kg/m^3)	Density range (1 σ) (kg/m^3)	DRE density used[a] (kg/m^3)	Percent vesicularity range	Number of clasts	Vesicularity classification[b]
Medium gray scoria	910	949	700–1200	2650	74–55	30	High-mod.
Light gray scoria	1060	1043	870–1210	2590	53–66	30	High-mod.
Dark gray dense	2530	2509	2270–2750	2750	17–0	30	Incip.-non
Medium gray dense	2460	2393	2170–2610	2620	17–0	30	Incip.-non
Light gray dense	2560	2455	2190–2710	2720	19–0	30	Incip.-non
Banded scoria	1500	1483	1240–1720	2650	53–35	30	Mod.-poor

All measured clasts from size fraction 9–64 mm (medium to coarse lapilli).
[a] Dense Rock Equivalent (DRE) densities used to calculate percent vesicularity are from Coombs et al., 2013.
[b] Vesicularity classes from Houghton and Wilson (1989, Table 2); mod., moderately vesicular, high, highly vesicular, incip., incipiently vesicular; poor, poorly vesicular; and non, non-vesicular.

small lava dome or plug. Although there is no direct evidence of dome growth between March 23 and March 26 (between events 6 and 7, Table 1), seismic tremor (Buurman et al., 2013), Forward Looking Infrared Radar (FLIR) temperatures (Wessels et al., 2013), and abundance of dense juvenile clasts in samples of event 8 deposit (March 26) imply that a dome probably existed. Event 8 had the greatest plume height of the eruption (18.9 km asl) which may also suggest vent plugging and pressurization by a lava dome. Satellite images and overflight observations of the presence or absence of a dome are inconclusive due to obscured conditions at the vent (Schaefer, 2012). No significant pyroclastic flows were identified, and if the presumed dome existed, it was likely small and thus a dome-collapse mechanism is unlikely to have initiated these events.

The origins of explosive events of March 26–28 (events 9–18, Table 1) are difficult to interpret due to infrequent direct observations during this time period and the fact that the 10 deposits are combined as a composite layer due to a lack of intervening snow layers. Deposit characteristics and geophysical data however, suggest that events 9–18 mark a change in eruptive character, somewhat distinct from earlier events and from the final event on April 4. Buurman et al. (2013) report a change in the character of seismicity prior to the explosive events 9–18 beginning with a very energetic swarm of earthquakes on March 26. Individual explosions were accompanied by lower frequency seismicity compared to events 1–6 which is consistent with the short duration explosions and high plume heights (Table 1). Infrasound data also show a shift in character from emergent to impulsive signals (Fee et al., 2013) which corroborate with seismic data. Sulfur dioxide emissions dropped significantly between March 25 and March 27 possibly suggesting a plugged vent (Lopez et al., 2013). No observations of the vent were made between March 26 and 28 owing to frequent explosions (10 explosive events in total) and a persistent low-level ash plume. A time-lapse camera positioned in the Drift River Valley captured images of small pyroclastic flows generated during events 11 and 15 (March 27 and 28 respectively) and small lahars generated during events 17 and 18 (March 28) (Schaefer, 2012, Figs. 15 and 16). Tephra-fall deposits from these explosions are among the finest grained deposits of the entire eruption (see Section 3.5). The composite layer of events 9–18 contains subequal proportions of vesicular and dense juvenile material similar to deposits of event 8, except for one that has noticeably less scoria (Fig. 12). No compositional data exist for these deposits because of their fine-grained character so we are not able to correlate a change in magma composition or texture to the notably finer grain-size or differences in seismic or infrasound data associated with these explosions. Deposits from events 9–18 are transitional in nature from earlier events (esp. 5, 6, and 8) to deposits of event 19 in that they contain relatively abundant scoriaceous clasts (e.g., earlier events) but are very fine grained (e.g., event 19). This may suggest that the eruption mechanism is transitional or a hybrid of multiple processes. Although not observed, it is possible that lava dome growth occurred between explosive blasts and the dense juvenile material found in these deposits is from fragmentation of those domes. We know that a dome was emplaced within a 10-hour time period on March 22 and the time lapses between explosions of events 9–18 range from 41 min to 12 h 21 min, ample time for dome extrusion. A continuous low-level ash plume during this time is consistent with growth and small-scale collapses of such domes. Small lahars and pyroclastic flows observed during this time also support partial dome collapses (Schaefer, 2012; Waythomas et al., 2013). Finer-grained deposits may be attributed to greater contribution of fine ash from elutriation of pyroclastic flows as well as hydro-magmatic interactions (i.e. efficient water-magma fragmentation) as evidenced by lahar generation. From these data we interpret explosive events 9–18 as hybrids of magmatically-driven explosions either initiated by plugging and pressurization of the vent by small domes or by collapse of domes accompanied by decompression-expansion of magma in the conduit. Continuous low-level activity between March 26 and 28 may indicate a steadier, continuous flow of magma to the surface compared to more punctuated events that came earlier where magma may have risen in smaller discrete batches.

The final explosive eruption on April 4 (event 19) is interpreted to result from collapse of the summit lava dome possibly punctuated by a small magmatically-driven explosion although it is unclear which process initiated the event. Between March 28 and April 4, a 36 to 44×10^6 m^3 dome was emplaced at the summit of Redoubt (Schaefer, 2012; Bull and Buurman, 2013). The explosion on April 4 (event 19, Table 1) resulted in significant tephra fall, a large lahar, and a small pyroclastic flow on the volcano's north flank (Waythomas et al., 2013; Bull and Buurman, 2013). The tephra-fall and pyroclastic-flow deposits are chiefly composed of dense juvenile material with ~2 wt.% vesicular material (Fig. 12B), suggesting largely degassed lava, consistent with fragmental dome rock. Juvenile clasts in the lahar deposit are nearly all relatively dense and commonly prismatically jointed, suggesting emplacement while hot (Waythomas et al., 2013). The grain-size of event 19 fall deposits is much finer than earlier deposits of similar volume and is likely attributed to hydro-magmatic interactions as evidenced by the large lahar of April 4 (Waythomas et al., 2013) as well as the contribution of fine ash from elutriation from the pyroclatic flow of April 4. These characteristics are similar to the "lithic-rich" tephras of 1990,

Fig. 10. Photographs of principal lithologies erupted during the explosive phase of the 2009 eruption of Redoubt Volcano. All components are from sample 09RDKLW093 erupted on March 23 during event 6 and are distinguished on the basis of color and texture. Insets are to show clast texture. A) Medium-gray low-silica andesite scoria. B) Light-gray intermediate- to high-silica andesite scoria. C) Dark-gray dense low-silica andesite. D) Medium-gray dense intermediate-to high-silica andesite. E) Light-gray intermediate-silica andesite. F) Banded scoria. G) Non-juvenile lithic clasts. Component density and mean percent vesicularity are given in Table 2. Whole rock analyses of most components are discussed in Coombs et al. (2013).

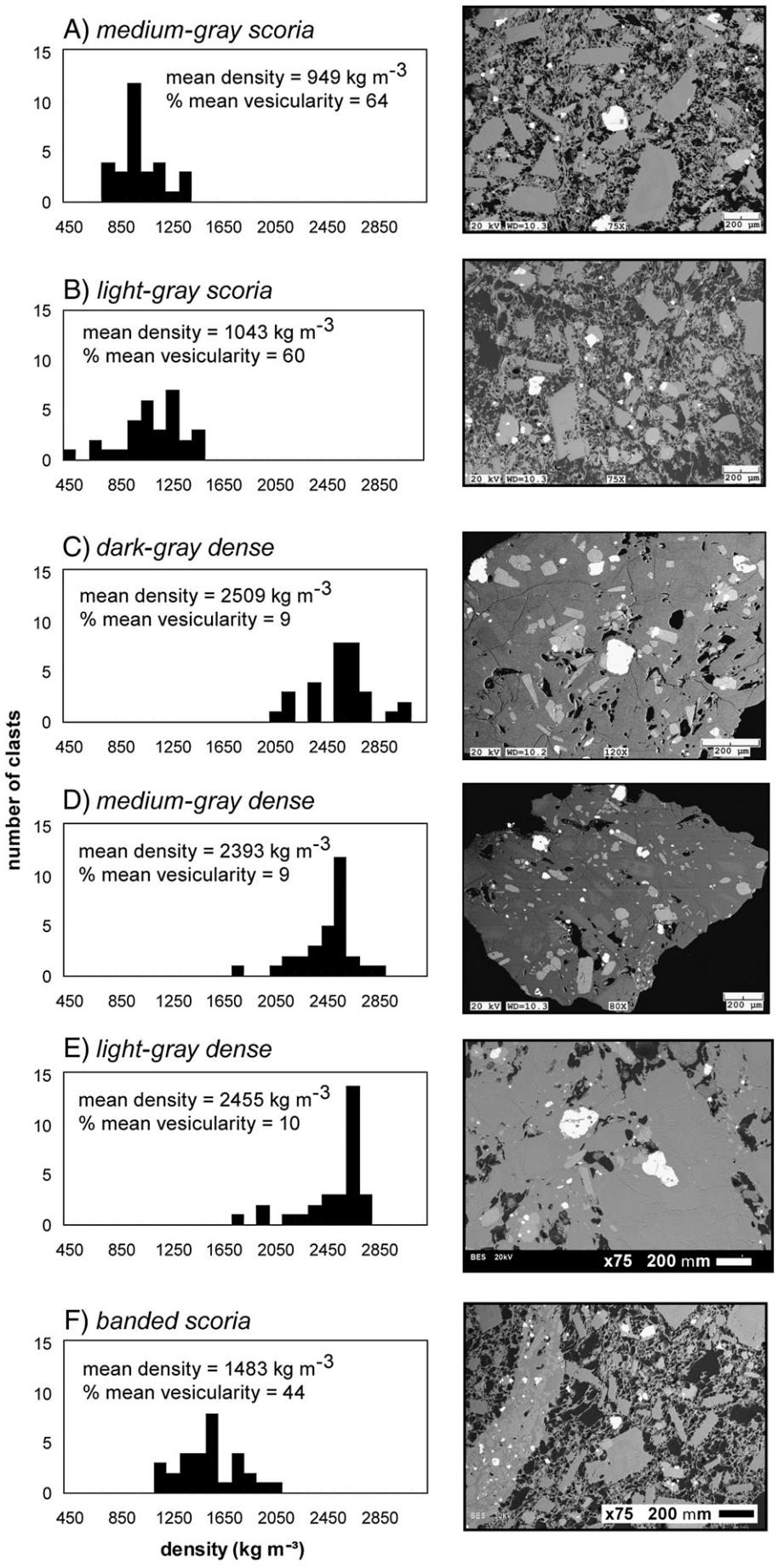
A) medium-gray scoria
mean density = 949 kg m-3
% mean vesicularity = 64
B) light-gray scoria
mean density = 1043 kg m-3
% mean vesicularity = 60
C) dark-gray dense
mean density = 2509 kg m-3
% mean vesicularity = 9
D) medium-gray dense
mean density = 2393 kg m-3
% mean vesicularity = 9
E) light-gray dense
mean density = 2455 kg m-3
% mean vesicularity = 10
F) banded scoria
mean density = 1483 kg m-3
% mean vesicularity = 44
number of clasts
density (kg m-3)
0 5 10 15
450 850 1250 1650 2050 2450 2850
x75 200 mm

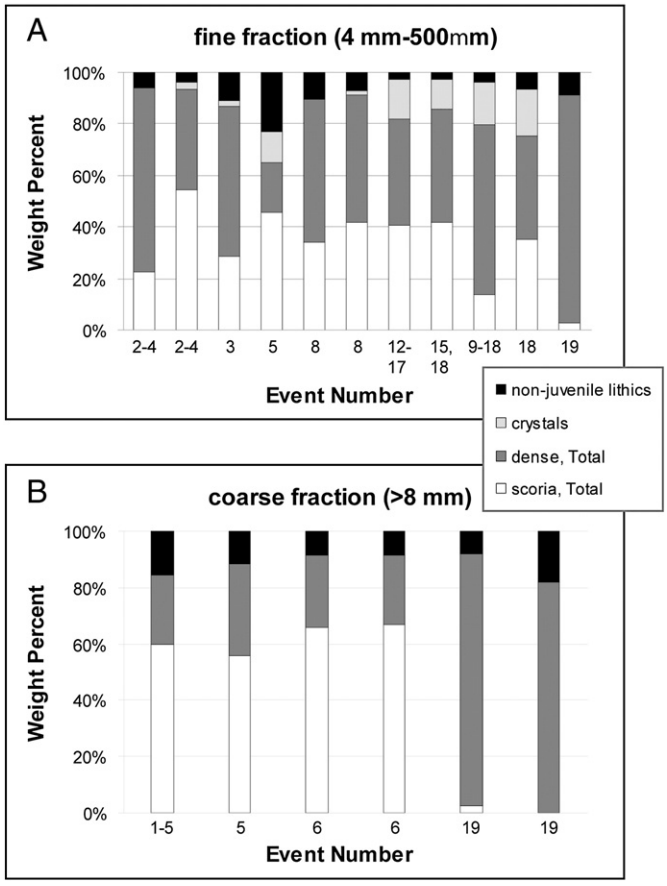

Fig. 12. Distribution of generalized component lithologies in each explosive event or event package. A) Componentry using fine-grained samples (4 mm–500 μm). B) Componentry using coarse-grained samples (≥8 mm). Componentry is given in weight percent not volume percent, and thus dense clasts may appear more abundant in these plots even if they are volumetrically smaller because they have a greater bulk density compared to vesicular clasts (see component densities in Table 3 and Fig. 11). We show componentry in generic terms "vesicular", "dense", "lithics", and "crystals" rather than by component lithologies show in Fig. 11 because compositional data was only possible for a few coarse-grained deposits. Free crystals are shown for fine-grained material only because they are not present in coarse-deposits. Refer to Section 2.4 for a discussion of methods for component analysis. Refer to Coombs et al. (2013) for compositional analyses of components.

attributed by Scott and McGimsey (1994) to generation from lithic pyroclastic flows caused by dome collapse.

A distinct change in magma composition is documented in April 4 deposits (Coombs et al., 2013). Juvenile lithic fragments that dominate the deposit are uniformly intermediate- to high-silica andesite composition (59–62 wt.%SiO_2) compared to the low-silica andesite composition (<58 wt.% SiO_2) that dominated events 1–6. This change in magma composition may have occurred as early as March 26 (event 7) but since no compositions were measured for event 7–18 deposits due to fine-grain size, we are not able to address the timing. Evolved matrix glasses, microlite-rich groundmass, and reaction rims on amphiboles are all suggestive of relatively slow ascent for the lava sampled from event 19 (Coombs et al., 2013).

Despite evidence that event 19 was dominated by a dome-failure mechanism; volume disparities between the pre-April 4 dome and event 19 fragmental deposits may suggest that some juvenile lava erupted during the event may have been conduit-derived. The volume of the lava dome at the summit prior to the explosion on April 4 is estimated at 36 to 44×10^6 m^3 (Diefenbach et al., 2013). The volume of event 19 pyroclastic-flow deposits are estimated to be 8.6×10^6 m^3 (Bull and Buurman, 2013) and the fall deposit is estimated to be 3.0×10^6 m^3 (this study). The lahar deposit contributes the greatest volume uncertainty, with estimates ranging from 60 to 250×10^6 m^3 (Waythomas et al., 2013). Estimates of the percentage of juvenile fragmental material in the April 4 lahar deposit do not exist. The solid fraction of the lahar is a composite of dome material and other materials incorporated during transport and cannot meaningfully be used to account for the total volume of the collapsed dome.

4.2. Particle aggregation

Exceptionally fine-grained fall deposits and the preponderance of associated particle aggregates are remarkable features of the 2009 Redoubt eruption. Particle aggregation is common in eruptions where magma–water interactions occur; where the energy budget of the ascending ash cloud is dominated by evaporative cooling and latent heat release from water phase changes causing highly efficient fragmentation which produces very fine particle sizes (Van Eaton et al., 2012). Aggregation occurs in the eruption column and the associated ash cloud dominantly through hydrometeor formation which incorporates fine ash particles and enhances fallout (e.g., Pruppacher and Klett, 1997). Sources of water include magmatic volatiles, entrained atmospheric moisture or external water during interaction between magma and sub-surface or above-surface water bodies (including ice). Conditions for particle aggregation were ideal during the 2009 eruption of Redoubt because it is a snow and ice-covered volcano providing an abundant source of external water and the eruption occurred at the end of winter, during maximum snow load. The 50–100 m thick Drift glacier that occupies the summit crater and possible melt water stored beneath the glacier are the mostly likely sources of external water (Waythomas et al., 2013). We attribute the origin of the exceptionally fine-grained particles that comprise aggregates as well as the aggregate themselves to hydro-magmatic interactions. In the previous section (see Section 4.1) we discuss the possible contribution of fine ash to deposits from elutriation from pyroclastic flows generated during explosions but we consider this a minor process compared to hydro-magmatic interactions.

The 2009 winter-time eruption of Redoubt provided an unparalleled opportunity to document particle aggregates (see Section 3.3) and associated disaggregated deposits (see Section 3.5) before they disappear from the geologic record so that (1) ash dispersion modelers may use these data to improve their ability to model ash cloud aggregation processes and, (2) future workers may better interpret these and prehistoric deposits. Typically (in the absence of aggregation), particle size decreases systematically with distance from source. Aggregation however, causes premature fallout of fine particles that would otherwise be entrained in the ash cloud and carried to more distal locations as individual particles. This is reflected in the poorly sorted character of disaggregated 2009 deposits (see Section 3.3 and 3.5; Fig. 13). Premature and non-systematic fallout of ash is clearly documented in the

Fig. 11. Clast density histograms of principal lithologic components erupted during the 2009 eruption of Redoubt Volcano. A) Dark-gray dense clasts; SEM image is of sample AGMcRDT004 (Table A.1). B) Medium-gray dense clasts; SEM image is of sample AGMcRDT004 (Table A.1). C) Light-gray dense clasts; SEM image is of sample 09RDMLC303B (Coombs et al., 2013). D) Medium-gray scoria clasts, SEM images of sample AGMcRDT004. E) Light-gray scoria; SEM image is of sample AGMcRDT004. F) Banded scoria; SEM image is from sample 09RDKLW001. All measured clasts are from size fraction 6–64 mm (fine to coarse lapilli). All components used to calculate density are from proximal sample 09RDKLW093 erupted on March 23 during event 6. Average percent vesicularity is calculated using the method of Houghton and Wilson (1989). Table 2 gives further data used for density and vesicularity measurements. SEM-backscatter electron photomicrographs of each component show microtextures; black areas are vesicles, gray areas are felsic phenocrysts and glass, and white areas are mafic phenocrysts. All scale bars are 200 μm.

high fraction of fine ash (up to 67 wt.%) especially in proximal locations (Fig. 14). We know from disaggregating sample 09RDKLW002C (Fig. 5A and B) that aggregates comprise a wide range of particle sizes. Frozen aggregate pellet deposits (prior to melting) in proximal locations were also often poorly sorted although far less so than their melted disaggregated counterparts (Fig. 5B and C). Aggregate pellets and ash clusters documented in distal locations are well sorted. This implies that once aggregates are formed in the eruption cloud, their fallout is more predictable or similar to sedimentation from dry volcanic eruptions where particle aggregation does not occur. The poorly sorted character of aggregate pellet sizes (esp. in proximal locations) probably results from variations in (1) growth history; (2) particle components

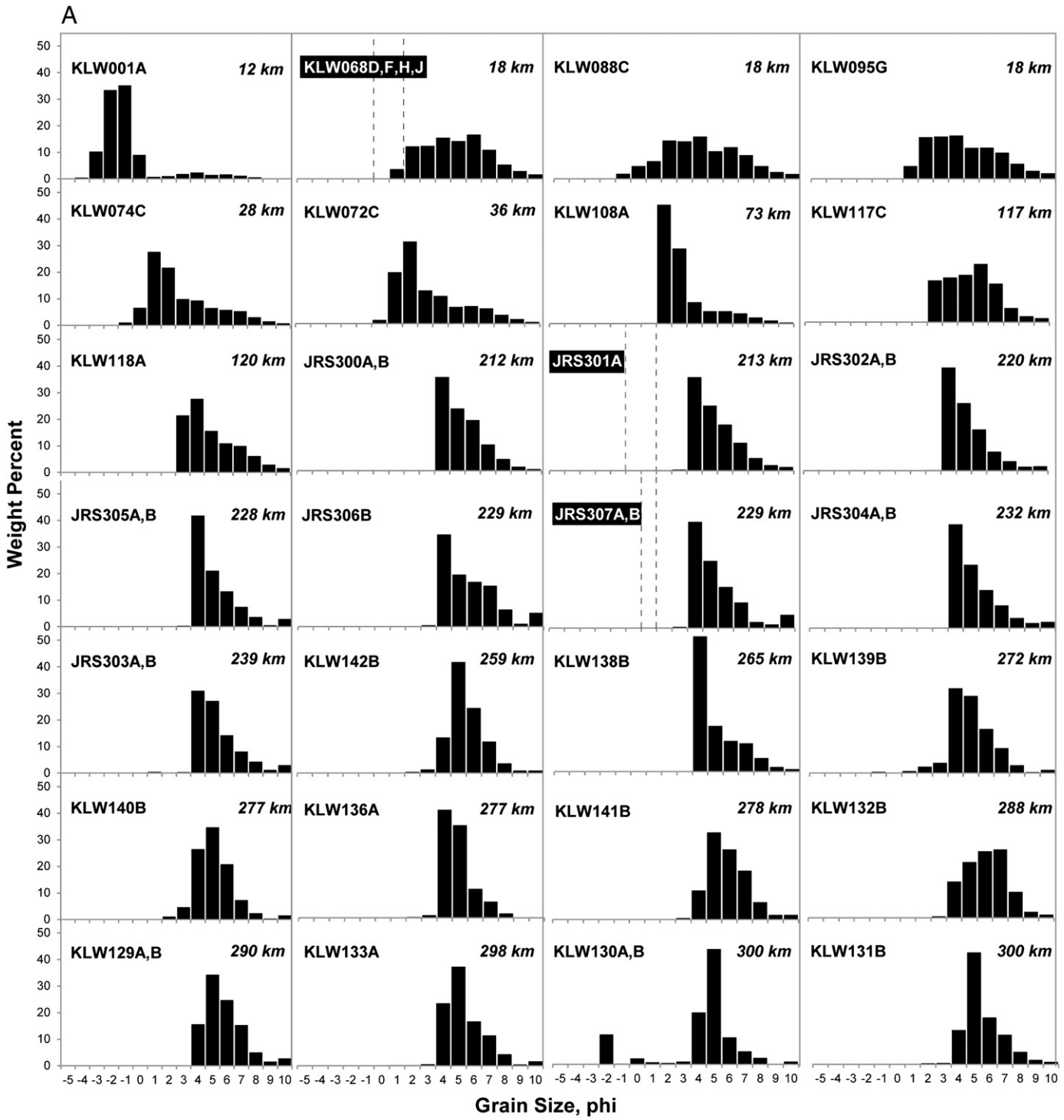

Fig. 13. Histograms of particle-size distribution of bulk tephra-fall deposits of the 2009 eruption at various distances downwind from Redoubt Volcano. A) Explosive event 5 on March 23, 2009 (Fig. 2). B) Explosive event 6 on March 23, 2009 (Fig. 2). C) Explosive event 19 on April 4, 2009 (Fig. 2). Histograms are aligned in order of distance from vent. All plots are shown at the same scale. Sample names, excluding the prefix "09RD" (omitted for brevity) and distance from source of each deposit are shown on each plot. Highlighted sample names are those in which aggregate pellet sizes in primary deposits were also measured in the field (dashed lines show size range of aggregates). Refer to Table A.2 for complete particle-size data. Phi of −5 to −1 are lapilli-size grains (2–32 mm) and phi of −1 to 10 are ash-size grains (2 mm–1 μm). Sample 09RDKFB321A of event 19 is from a pyroclastic flow.

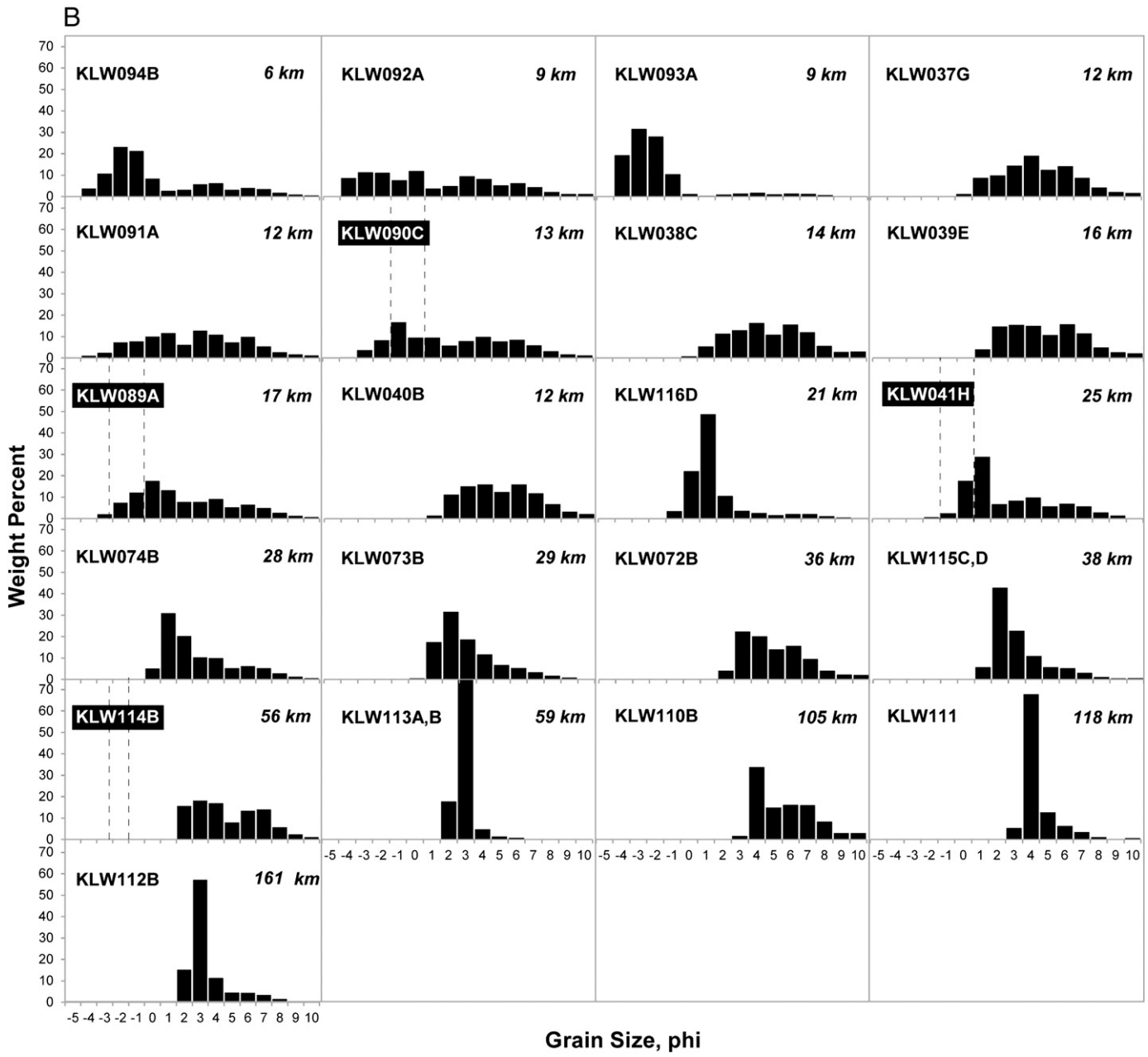

Fig. 13 (*continued*).

(liberated crystals, vesicular and lithic fragments, each with varying density, shape and size); (3) fragmentation mechanisms (vesiculation, interaction with external water, vent erosion, etc.); and (4) size-dependent sorting mechanisms (turbulent transport, particle aggregation, hydrometer formation, and gravitational settling) (Wohletz et al., 1989).

Future work on 2009 deposits and other historical and prehistoric eruptions of Redoubt should be approached with the knowledge that conditions for particle aggregation are likely a dominant process. Similar accretionary pellets are documented in historical eruptions (Scott and McGimsey, 1994) and evidence such as very fine-grained, poorly-sorted, proximal deposits have been observed by the senior author in many prehistoric tephra deposits from this volcano. Due to the significant amount of water (ice) contained in the aggregates and subsequent melting into muddy deposits, preservation potential is poor. Because aggregates were volumetrically significant in all deposits, we again emphasize that the particle size data shown in this paper (see Section 3.5) are of disaggregated samples and do not represent the original size distribution found in deposits at the time of deposition. This will pose significant challenges to those using this dataset to model cloud dynamics including tephra dispersion and fallout. Mastin et al. (2013) for example use an ash plume and sedimentation model (Ash3D) to replicate event 5 on March 23. They report having to modify input eruption parameters several times before they produced model output that reasonably matched the isomass contours reported in this paper.

4.3. Significance and hazards of tephra-fall deposits

4.3.1. Comparison with the 1989–90 eruption and other sources

The 2009 eruption of Redoubt was generally similar to the 1989–90 Redoubt eruption in terms of magma composition, plume heights, mass/volumes of individual tephra-fall deposits, duration of explosive events, and production of frozen aggregate lapilli (Scott

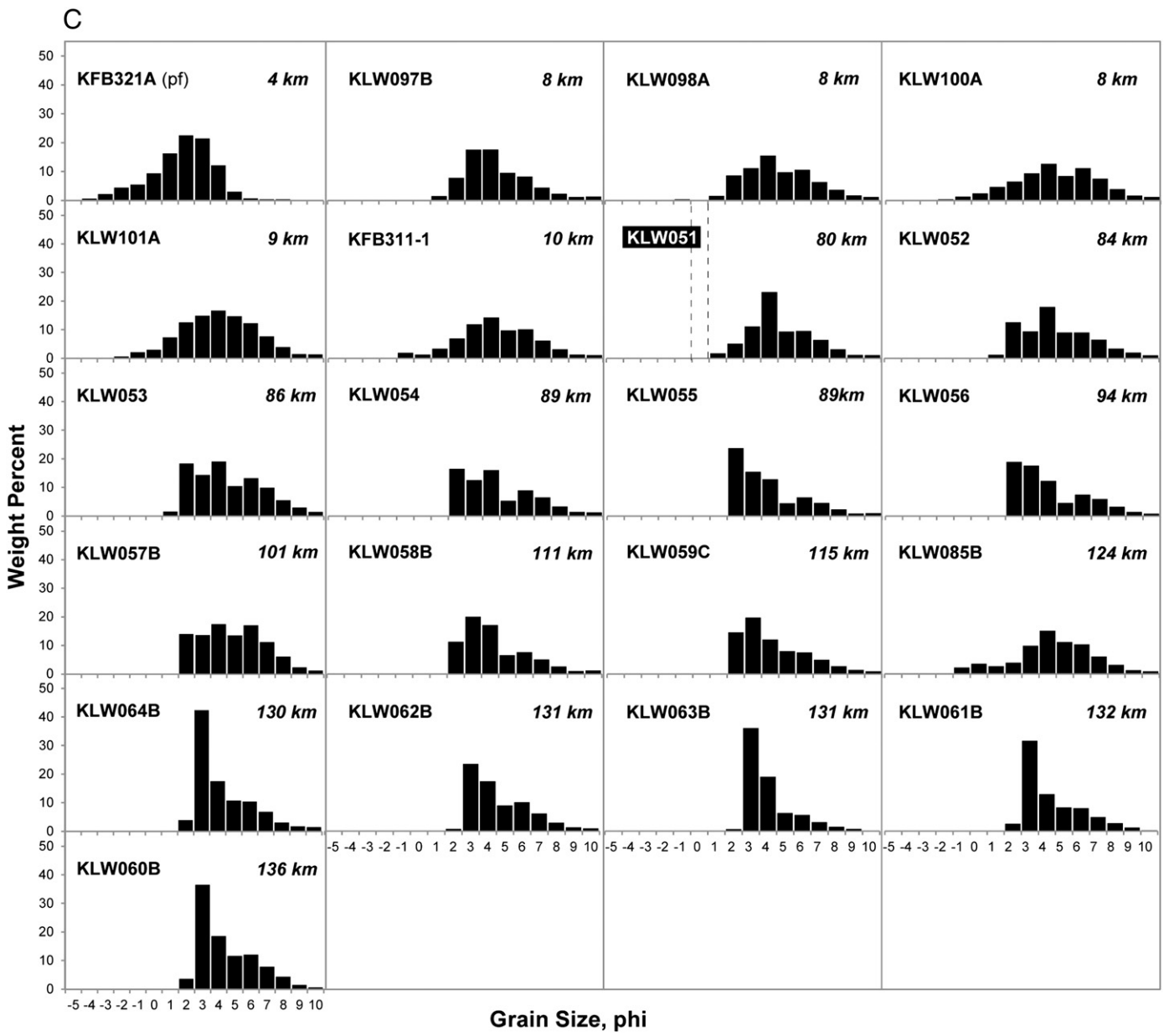

Fig. 13 (*continued*).

and McGimsey, 1994). The main difference between the two eruptions is fewer significant dome-collapse events and pyroclastic flows during the 2009 eruption. Such events contributed significantly to the total eruption mass as well as mass of tephra-fall deposits (esp. fine ash) in 1989–90 (Scott and McGimsey, 1994). Fine ash produced in the 2009 eruption is attributed mainly to magma–water interactions through hydro-magmatic processes and far less so to elutriation from pyroclastic flows. Other differences include larger lahars but fewer and smaller volume domes in 2009 (Waythomas et al., 2013). Both eruptions were assigned a composite Volcanic Exclusivity Index (VEI) of 3 (Venzke et al., 2002 and personal communication with L. Siebert, 2009) and mass and volume of individual tephra-fall events are similar for those originating as magmatically-driven explosions (rather than as co-pyroclastic-flow fall out) (Scott and McGimsey, 1994). Table 4 shows a comparison of 2009 Redoubt tephra-fall deposits with those of other historical events. The 2009 eruption is comparable with other Cook Inlet eruptions within an order of magnitude, in particular the 1986 and 2006 eruptions of Augustine and the 1992 eruption of Crater Peak.

4.3.2. Hazards

Hazards from volcanic ash are considered two-fold, those from drifting ash clouds and those from ash fall on communities and infrastructure. Drifting ash clouds are a primary concern to aviation because ingestion of ash by jet engines can result in engine failure as occurred during the 1989–90 eruption of Redoubt (Miller and Casadevall, 2000). AVO works closely with the Federal Aviation Administration (FAA) and the National Weather Service (NWS) to provide ample warning of an impending eruption so that aviation encounters can be prevented. Timely issuance of flight restrictions and severe weather warnings by these agencies mitigate hazards to aviators (Schaefer, 2012). The potential threat of ash fall on communities was a significant concern during the 2009 Redoubt eruption based on known impacts from historical eruptions of Redoubt and other Cook Inlet volcanoes (e.g., Brantley, 1990; Miller et al., 1998; Scott and McGimsey, 1994; McGimsey et al., 2001). Primary hazards associated with ash fall on communities include closure of critical infrastructure (airports, power supply plants, etc.), air and water quality perturbations, decreased visibility, and mechanical abrasion and corrosion to machinery. Satellite

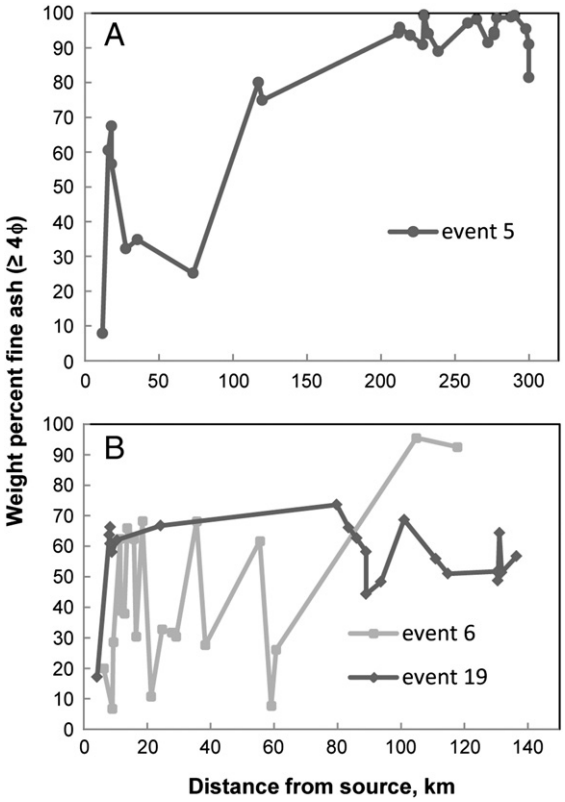

Fig. 14. Plots showing weight percent fine ash (≥4ϕ; ≥63 μm) in 2009 tephra-fall deposits with distance from the vent. A) Event 5. B) Events 6 and 19.

imagery, National Oceanic and Atmospheric Administration (NOAA) Hybrid Single-Particle Lagrangian Integrated Trajectory (HYSPLIT) wind-model data, ash-plume and fall modeling, and coordination with the NWS (the agency responsible for issuing ashfall advisories) aided AVO in tracking and projecting ash-plume movement and, furthermore, assisted us in briefing the public about the likelihood and nature of tephra fall throughout the eruption. The long period of unrest preceding the explosive eruptions led to significant public warnings and preparations by lifeline organizations (e.g., Department of Environmental Conservation, Division of Homeland Security and Emergency Management). Ash fall preparedness information is available and advertised to the public via many agency partners. AVO coordinates with local and state agencies to inform the public on impacts to air and water quality and general health-related issues, should they occur.

4.3.3. Impacts from tephra fall

Impacts from the drifting ash clouds and ash fall on communities were relatively minor mostly owing to mitigation measures taken by AVO and interagency partners. Drifting ash clouds as well as the threat of ash fall caused major disruptions to the aviation industry although no significant encounters were reported. Throughout the 2009 eruption, nearly 300 flights were canceled, some 60 were rerouted, 20 diverted, and 10 turn-backs; affecting more than 20,000 passengers (Murray et al., 2009). Economic impacts due to reroutes of air cargo flights away from Anchorage as well as personnel layoffs occurred in response to volcanic ash fall at the Ted Stevens International Airport in Anchorage, Alaska's largest city. Military aviation operations were impacted in response to the threat of ash fall on military bases in Anchorage by moving aircraft and personnel to other military bases (Schaefer, 2012).

Owing to the fact that most populated communities are located more than 80 km from the volcano, significant ash fall on communities was not expected. Heavy tephra fall (generating deposits up to 5 cm thick) occurred within 15 km of the volcano and posed minimal hazards because this area was unpopulated. Minor ash deposits (0.8–2.0 mm) occurred in communities along the Kenai Peninsula (80–100 km ESE), Anchorage (170 km NE) and Silver Salmon Creek Lodge (48 km S, on the western Cook Inlet). Trace ash deposits (<0.8 mm) were reported as far as Fairbanks (550 km) NNE of the volcano. As the eruption occurred during winter months, most ash fell on snow. The thin dark-colored deposits absorbed solar radiation and accelerated snow melting at the surface which effectively wetted and "locked" in the fine ash particles, and thus prevented significant reworking of the ash. Snow falls that buried ash-fall deposits, also prevented resuspension of ash. In the weeks following ash fall, spring temperatures melted the ash-bearing snow and the ash was washed away in meltwater streams and was not typically resuspended. In areas where snow was not present during ash fall (city streets, sidewalks, etc.), fine ash was a nuisance to clean up and resuspension occurred (Fig. 17). Glaciers in south-central Alaska received trace to minor ash falls (≤1 mm) which accelerated snow and ice melt due to increased solar absorption (event 17, March 28; Fig. 16, Louis Sass, USGS, personal communications, 2010). Relatively short eruption durations (<1 to 30 min) meant that ash fall on urban and rural communities was also short lived, lasting no more than 1.5 h (April 4) but, more commonly, 10 to 30 min. Early morning or late night ash fall events (March 23, April 4) caused fewer impacts to communities because of lack of direct exposure to falling ash.

Impacts to communities were relatively minor and more of a distraction and nuisance than a hazard, although economic losses due to disruptions to airline travel were significant (Schaefer, 2012). Preparedness activities by communities and individuals significantly reduced ground-based impacts (e.g., remaining indoors during ash fall, covering electronics and engine parts, suspending outdoor activities during ash fall, wearing dust masks during clean up, etc.). South-central Alaska organizations from small-town fire stations to whole city governments publicized emergency ash fall plans by early February. Local stores stocked up on emergency supplies (dust masks, air filters, bottled water, goggles, etc.) and sold out periodically. Nonetheless, impacts to local commerce were felt; some positive and some negative. Significant shipping delays caused by airline flight cancelations resulted in a number of stock shortages at local stores including food supply and floral deliveries. Businesses trading in preparedness and clean up supplies or services experienced retail booms. Stranded travelers caused short-term booms in businesses including rental cars, hotels, and restaurants.

Health-related impacts from ash fall were relatively minor. Closures of area clinics during ash fall in Homer on March 26 caused a spike in emergency room visits unrelated to ash fall. Other than complaints of itchy eyes and raspy throats, there was no significant increase in ash-related respiratory ailments in Anchorage during the March 28 ash fall event. Worried pet owners kept veterinary clinic phone lines busy (VCA Animal Hospitals, personal communications, 2009). Ash leachate analyses performed at the AVO using the methods of Hageman (2007) showed that leachable chemicals adsorbed onto the surface of ash particles, were not a significant concern to human or environmental health as they did not exceed local water quality standards. Air-quality samplers of fine particulate matter (PM) operated by the Municipality of Anchorage (MOA) and the Department of Environmental Conservation as well as the US Fish and Wildlife Service detected elevated levels of PM10 and PM2.5 (<10 and 2.5 μm, respectively) in Anchorage (Mar 28) and Soldotna (Mar 26), during the eruption (personal communication with Matt Stichick, MAO—Division of Air Quality, April 17). Particles 10 μm (that is, PM10) in diameter and smaller can be harmful if inhaled into the respiratory tract. Fine particulate levels spiked to 289 μg/m^3 at 17:00 AKDT in Anchorage on March 28, exceeding the Environment Protection Agency 24-hour

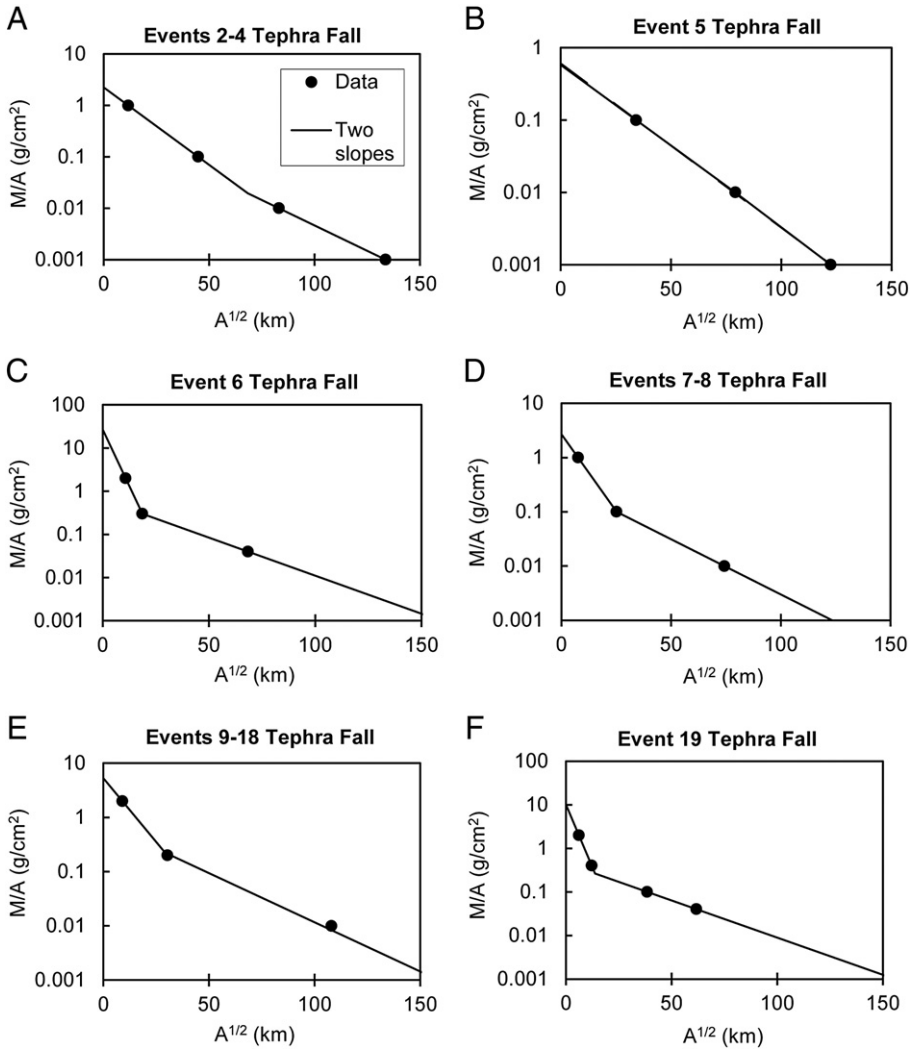

Fig. 15. Plots showing mass-per-unit area (MPUA) versus the square root of isomass area for deposits of tephra fall events (Table 1) of the 2009 eruption of Redoubt Volcano. Uncertainties in mass estimates reflect the fitting of a straight line (single slope line) or two linear segments (two-slope line). Our data are best fitted to two-slope line for all estimates except event 5 which is best fitted to a single-slope line. Tephra volume is calculated from the total mass of the deposit using the root-area method (Pyle, 1989; Fierstein and Nathenson, 1992).

particulate air quality standard (150 μg/m^3). Two other periods of elevated PM10 and PM2.5 were measured in Anchorage on March 31 and April 1 (up to 229 μg/m^3 for PM_{10}) and are thought to be associated with resuspension of ash from roadways from the March 28 ash fall deposit (event 17). Air quality standards were otherwise not exceeded (where monitored) during the 2009 eruption.

The most significant ash fall events in terms of ground-based impacts occurred on March 26 and 28 and April 4, mainly because ash was deposited in a broad swath from Seldovia, across the entire Kenai Peninsula to Anchorage, the most populous region in Alaska. On the afternoon of March 28, drifting ash clouds and ash fall in Anchorage resulted in the closure of the Ted Stevens International

Table 4
Comparison of 2009 Redoubt tephra-fall deposits with those of other historical events. Total volumes represent the sum of multiple tephra-fall events that occurred over a period of days to months.

Volcano–date	Total erupted mass ($\times 10^{10}$ kg)	Volume of individual fall deposits ($\times 10^6$ m^3)	Total volume of combined fall deposits ($\times 10^6$ m^3)	VEI	Reference
Redoubt–2009	5.5	4.4–15.1 (B); 1.7–5.7 (DRE)	54.6 (B); 20.6 (DRE)	3	1
Redoubt–1989–1990	8–13	0.04–20 (DRE)	40.0 (DRE)	3	2
Augustine–2006	2.2	0.4–4.6 (B); 0.2–1.8 (DRE)	22.0 (B); 8.5 (DRE)	3	3
Augustine–1986	7	0.1–26.4 (DRE)	26.4 (DRE)	4	4
Spurr/Crater Peak–1992	10.6	44–56 (B); 12–15 (DRE)	152 (B); 41 (DRE)	4	5
Nevado del Ruiz, Columbia, 1985	nd	15 (DRE)	15(DRE)	3	6
Mount St. Helens–1980	58	200 (DRE)	1100 (B); 200 (DRE)	5	7

B, bulk tephra volume; DRE, Dense Rock Equivalent tephra volume; VEI, Volcanic Explosivity Index; and nd, no data.
References: 1, this report; 2, Scott and McGimsey (1994); 3, Wallace et al. (2010); 4, Pyle (2000); 5, McGimsey et al. (2001); 6, Calvache (1990); and 7, Sarna-Wojcicki et al. (1981).

Fig. 16. Photograph showing the effects of minor ash fall (≤1 mm) on the Eklutna Glacier near Anchorage, Alaska, from the 2009 eruption of Redoubt Volcano. Snow melt was accelerated by solar absorption of the dark-colored ash-fall deposit on the surface. The lumpy surface was noted by researchers studying this glacier but also by many mountaineers in the area. Photograph by Louis Sass, USGS.

Airport for nearly 20 h. Although the April 4 ash fall event affected a relatively narrow swath of the lower Kenai Peninsula from Anchor Point to Seldovia, up to 2 mm of ash (the thickest reported ash fall on a population center) was deposited on dry surfaces (due to spring melt out of snow) causing longer term impacts due to reworking of the ash by wind, clean up, and normal activities (Fig. 17).

5. Conclusions

The 2009 eruption of Redoubt Volcano was similar to its previous historical eruptions. Magmatic explosions along with dome-building and collapse are common at this volcano. In addition to voluminous lahars, tephra plumes and tephra fall out are the primary hazards at this volcano. Key findings from this study include:

Fig. 17. Photograph showing active reworking of ash-fall deposit on a paved roadway in Nikiski, Alaska. Reworking of ash fall occurs days to months after deposition and affects air quality which poses health hazards if there is long-term exposure.

(1) The 2009 eruption comprised a series of 20 short-duration (<1–31 min) tephra-producing explosions with plume heights between 5.2 and 19 km asl erupted over a 21 day period (Mar 15–April 4) and were distributed downwind along nearly all azimuths of the volcano.
(2) We estimate the total mass of tephra-fall deposits at 54.6×10^9 kg with a total DRE volume of 20.6×10^6 m^3; similar to the last eruption of Redoubt in 1989–90 (Scott and McGimsey, 1994).
(3) Hydro-magmatic interactions (magma–water) are considered the primary cause of tephra-producing plumes. Plugging of the vent by small lava domes likely pressurized the system leading to explosive events (magmatically-driven). Only one tephra-producing plume was attributed to the gravitational collapse of a summit dome (event 19—April 4), a process that was much more common in the 1989–90 eruption (Scott and McGimsey, 1994).
(4) Ash aggregates comprise a significant volume of the tephra, and are ubiquitous in all deposits regardless of origin (e.g., dome collapse, magmatic explosion), size of explosion (plume height, duration), or distance from source.
(5) Particle size data showing a preponderance of fine ash, even in the most proximal locations suggests that particle aggregation processes caused premature fall out of fine ash.
(6) A winter-time eruption provided an unparalleled opportunity to document primary deposits (incl. frozen aggregates and discrete layers) preserved in the snow pack. Within a month of the eruption, tephra-fall layers coalesced into a single composite layer on the landscape and lack any evidence of having originated as multiple deposits or as layers comprised dominantly of ash aggregates.
(7) Minor ash deposits (0.8–2.0 mm) occurred in communities along the Kenai Peninsula (80–100 km ESE) and Anchorage (170 km NE). Trace ash deposits (<0.8 mm) were reported as far as Fairbanks (550 km) NNE of the volcano.
(8) Impacts to communities were relatively minor and more of a distraction and nuisance than a hazard, although economic losses due to disruptions to airline travel were significant.

Supplementary data to this article can be found online at http://dx.doi.org/10.1016/j.jvolgeores.2012.09.015.

Acknowledgments

We would like to thank the Alaska Volcano Observatory staff and visiting scientists who helped during the response to the 2009 eruption. We thank Kate Bull, Angie Diefenbach, Allana Drossos, Steve Schilling, Game McGimsey, Roger Dinlinger, and Colby Wallace for assisting in the field. Our hats are off to the many “citizen scientists” living in South Central Alaska for their keen observations and sampling efforts made during the eruption. We thank Dave Schneider for assistance in acquiring radar data for use in mapping tephra deposits. We thank Janelle Dyer, Allison Payne, Simone Girst, and Elisabeth Faulk for assistance in the Tephra Laboratory processing samples. Information on ash fall impacts came from a number of sources including news stories that could not be properly cited thus we acknowledge the Alaska Superstation, the Anchorage Daily News, Elmendorf Air Force Base, The Homer Tribune, The Fairbanks News Miner, and The Peninsula Clarion for their news reports. Finally, we thank Willie Scott and Adam Durant for their thoughtful and constructive reviews that improved the manuscript.

References

Beget, J.E., Nye, C.J., 1994. Postglacial eruption history of Redoubt volcano, Alaska. In: Miller, T.P., Chouet, B.A. (Eds.), The 1989–1990 Eruptions of Redoubt Volcano, AlaskaJournal of Volcanology and Geothermal Research 62, 31–54.
Brantley, S.R. (Ed.), 1990. The Eruption of Redoubt Volcano, Alaska, December 14, 1989–August 31, 1990: U.S. Geological Survey Circular C, 1061. 33 pp.
Brown, R.J., Bonadonna, C., Durant, A.J., 2012. A review of volcanic ash aggregation. Journal of Physics and Chemical of the Earth 45–46, 65–78.
Bull, K.F., Buurman, H., 2013. An overview of the 2009 eruption of Redoubt Volcano, Alaska. Journal of Volcanology and Geothermal Research 259, 2–15.
Bull, K.F., Anderson, S.W., Diefenbach, A.K., Wessels, R.L., Henton, S.M., 2013. Emplacement of the final lava dome of the 2009 eruption of Redoubt Volcano, Alaska. Journal of Volcanology and Geothermal Research 259, 334–348.
Buurman, H., West, M.E., Thompson, G., 2013. The seismicity of the 2009 Redoubt eruption. Journal of Volcanology and Geothermal Research 259, 16–30.
Calvache, V.M.L., 1990. Geology and volcanology of the recent evolution of Galeras volcano, Colombia. Unpublished MSci thesis, Louisiana State Univ, 172 pp.
Carey, S., Sparks, R.S.J., 1986. Quantitative models of the fallout and dispersal of tephra from volcanic eruptions clouds. Bulletin of Volcanology 48 (2–3), 109–125.
Casadevall, T.J., Doukas, M.P., Neal, C.A., McGimsey, R.G., Gardner, C.A., 1994. Emission rates of sulfur dioxide and carbon dioxide from Redoubt Volcano, Alaska during the 1989–1990 eruptions. In: Miller, T.P., Chouet, B.A. (Eds.), The 1989–1990 Eruptions of Redoubt Volcano, AlaskaJournal of Volcanology and Geothermal Research 62, 519–530.
Chough, S.K., Sohn, Y.K., 1990. Depositional mechanics and sequences of base surges, Songaskan tuff rings, Cheju Island, Korea. Sedimentology 37, 1115–1135.
Coombs, M.L., Sisson, T.W., Bleick, H.A., Henton, S.M., Nye, C.J., Payne, A.L., Cameron, C.E., Larsen, J.F., Wallace, K.L., Bull, K.F., 2013. Andesites of the 2009 eruption of Redoubt Volcano, Alaska. Journal of Volcanology and Geothermal Research 259, 349–372.
Diefenbach, A.K., Bull, K.F., Wessels, R.L., McGimsey, R.G., 2013. Photogrammetric monitoring of lava dome growth during the 2009 eruption of Redoubt Volcano. Journal of Volcanology and Geothermal Research 259, 308–316.
Dorava, J.M., Waythomas, C.F., 1995. Hydrologic hazards at recently active volcanoes in the Cook Inlet Region, Alaska. In: Herrman, R. (Ed.), Annual Summer Symposium—1995, Water Resources and Environmental Hazards: Emphasis on Hydrologic and Cultural Insight in the Pacific Rim, Honolulu, HI. American Water Resources Association, pp. 91–98.
Fee, D., McNutt, S.R., Lopez, T.M., Arnoult, K.M., Szuberla, C.A.L., Olson, J.V., 2013. Combining local and remote infrasound recordings from the 2009 Redoubt Volcano eruption. Journal of Volcanology and Geothermal Research 259, 100–114.
Fierstein, J., Nathenson, M., 1992. Another look at calculation of fallout tephra volumes. Bulletin of Volcanology 54, 156–167.
Fisher, R.V., 1961. Proposed classification of volcaniclastic sediments and rocks. Geological Society of America Bulletin 72, 1409–1414.
Hageman, P.L., 2007. U.S. Geological Survey field leach test for assessing water reactivity and leaching potential of mine wastes, soils, and other geologic and environmental materials. U.S. Geological Survey Techniques and Methods Report 5-D3. http://pubs.usgs.gov/tm/2007/05D03/pdf/TM5-D3_508.pdf.
Houghton, B.F., Wilson, C.J.N., 1989. A vesicularity index for pyroclastic deposits. Bulletin of Volcanolology 51, 451–462.
Lopez, T., Carn, S., Werner, C., Fee, D., Kelly, P., Doukas, M., Pfeffer, M., Webley, P., Cahill, C., Schneider, D., 2013. Evaluation of Redoubt Volcano's sulfur dioxide emissions by the Ozone Monitoring Instrument. Journal of Volcanology and Geothermal Research 259, 290–307.
Mastin, L.G., Guffanti, M., Servranckx, R., Webley, P., Barsotti, S., Dean, K., Durant, A., Ewert, J.W., Neri, A., Rose, W.I., Schneider, D., Siebert, L., Stunder, B., Swanson, G., Tupper, A., Volentik, A., Waythomas, C.F., 2009. A multidisciplinary effort to assign realistic source parameters to models of volcanic ash-cloud transport and dispersion during eruptions. Journal of Volcanology and Geothermal Research 186, 10–21. http://dx.doi.org/10.1016/j.jvolgeores.2009.01.008.
Mastin, L.G., Schwaiger, H., Schneider, D.J., Wallace, K.L., Schaefer, J., Denlinger, R.P., 2013. Injection, transport, and deposition of tephra during event 5 at Redoubt Volcano, 23 March, 2009. Journal of Volcanology and Geothermal Research 259, 201–213.
McGimsey, R.G., Neal, C.A., Riley, C.M., 2001. Areal distribution, thickness, mass, volume, and grain size of tephra-fall deposits from the 1992 eruptions of Crater Peak Vent, Mt. Spurr volcano, Alaska. U.S. Geological Survey Open-File Report 01-0370. 38 pp.
McNutt, S.R., Thompson, G., West, M.E., Fee, D., Stihler, S., Clark, E., 2013. Local seismic and infrasound observations of the 2009 explosive eruptions of Redoubt Volcano, Alaska. Journal of Volcanology and Geothermal Research 259, 63–76.
Miller, T.P., Casadevall, T.J., 2000. Volcanic ash hazards to aviation. In: Sigurdsson, Haraldur (Ed.), Encyclopedia of Volcanoes. Academic Press, San Diego, pp. 915–930.
Miller, T.P., Chouet, B.A., 1994. The 1989–1990 eruptions of Redoubt volcano: an introduction. In: Miller, T.P., Chouet, B.A. (Eds.), The 1989–1990 Eruptions of Redoubt Volcano, Alaska: Journal of Volcanology and Geothermal Research, 62 (1), pp. 1–10.
Miller, T.P., McGimsey, R.G., Richter, D.H., Riehle, J.R., Nye, C.J., Yount, M.E., Dumoulin, J.A., 1998. Catalog of the historically active volcanoes of Alaska. U.S. Geological Survey Open-File Report 98-0582, 104.
Murray, J.J., Matus, A.V., Hudnall, L.A., Krueger, A.J., Haynes, J.A., Pippin, M.R., 2009. Volcanic ash impacts on air traffic from the 2009 Mt. Redoubt eruption. Eos Transactions, America Geophysical Union 90 (52) (Fall Meeting Supplement, Abstract V31A-1949).
Power, J.A., Stihler, S.D., Chouet, B.A., Haney, M.M., Ketner, D.M., 2013. Seismic observations of Redoubt Volcano, Alaska — 1989–2010 and a conceptual model of the Redoubt magmatic system. Journal of Volcanology and Geothermal Research 259, 31–44.
Pruppacher, H.R., Klett, J.D., 1997. Microphysics of Clouds and Precipitation, Second Revised and Enlarged Edition with an Introduction to Cloud Chemistry and Cloud Electricity. Kluwer Academic Publishers, Dordrecht, p. 954.
Pyle, D.M., 1989. The thickness, volume, and grain size of tephra-fall deposits. Bulletin of Volcanology 51, 1–15.
Pyle, D.M., 2000. Sizes of volcanic eruptions. In: Sigurdsson, H., Houghton, B.F., McNutt, S.R., Rymer, H., Stix, J. (Eds.), Encyclopedia of Volcanoes. Academic Press, San Diego, CA, pp. 263–269.

Sarna-Wojcicki, A.M., Shipley, S., Waitt, R.B., Dzurisin, D., Wood, S.H., 1981. Areal distribution, thickness, mass, volume, and grain size of air-fall ash from six major eruptions of 1980. In: Lipman, P.W., Mullineaux, D.R. (Eds.), The 1980 Eruptions of Mount St. Helens, Washington: U.S. Geological Survey Professional Paper 1250, pp. 577–600.

Schaefer, J.R. (Ed.), 2012. The 2009 Eruption of Redoubt Volcano, Alaska, Alaska Division of Geological and Geophysical Surveys Report of Investigations 2011-5, p. 45.

Schaefer, J.R., Wallace, K.L., 2012. Ash fall contour map of the 2009 eruption of Redoubt Volcano, Alaska: digital shapefiles of contours and sample locations. Alaska Division of Geological and Geophysical Surveys, Miscellaneous Publication 143, 1 DVD.

Schmid, R., 1981. Descriptive nomenclature and classification of pyroclastic deposits and fragments: recommendations of the IUGS Subcommission on the Systematics of Igneous Rocks. Geology 9, 41–43.

Schneider, D.J., Hoblitt, R.P., 2013. Doppler weather radar observations of the 2009 eruption of Redoubt Volcano, Alaska. Journal of Volcanology and Geothermal Research 259, 133–144.

Scott, W.E., McGimsey, R.G., 1994. Character, mass, distribution, and origin of tephra-fall deposits of the 1989–1990 eruption of Redoubt Volcano, south-central Alaska. Journal of Volcanology and Geothermal Research 62, 251–272.

Steensen, T., Stuefer, M., Webley, P., Grell, G., Freitas, S., 2013. Qualitative comparison of Mount Redoubt 2009 volcanic clouds using the PUFF and WRF-Chem dispersion models and satellite remote sensing data. Journal of Volcanology and Geothermal Research 259, 235–247.

Van Eaton, A.R., Herzog, M., Wilson, C.J.N., McGregor, J., 2012. Ascent dynamics of large phreatomagmatic eruption clouds: the role of microphysics. Journal of Geophysical Research 117, B03203. http://dx.doi.org/10.1029/2011JB008892.

Venzke, E., Wunderman, R.W., McClelland, L., Simkin, T., Siebert, L., Mayberry, G. (Eds.), 2002. Global Volcanism, 1968 to Present: Smithsonian Institution, Global Volcanism Program Digital Information Series GVP-4. http://www.volcano.si.edu/world/reports/.

Walker, G.P.L., 1981. Plinian eruptions and their products. Bulletin of Volcanology 44, 223–240.

Wallace, K.L., Neal, C.A., McGimsey, R.G., 2010. Timing, distribution, and character of tephra fall from the 2005–2006 eruption of Augustine Volcano. In: Power, J.A., Coombs, M.L., Freymueller, J.T. (Eds.), The 2006 Eruption of Augustine Volcano, Alaska: U.S. Geological Survey Professional Paper 1769, pp. 187–217. http://pubs.usgs.gov/pp/1769/chapters/p1769_chapter09.

Waythomas, C.F., Pierson, T.C., Major, J.J., Scott, W.E., 2013. Voluminous ice-rich and water-rich lahars generated during the 2009 eruption of Redoubt Volcano, Alaska. Journal of Volcanology and Geothermal Research 259, 389–413.

Webley, P.W., Lopez, T.M., Ekstrand, A.L., Dean, K.G., Rinkleff, P., Dehn, J., Cahill, C.F., Wessels, R.L., Bailey, J.E., Izbekov, P., Worden, A., 2013. Remote observations of eruptive clouds and surface thermal activity during the 2009 eruption of Redoubt volcano. Journal of Volcanology and Geothermal Research 259, 185–200.

Werner, C., Kelly, P.J., Doukas, M., Lopez, T., Pfeffer, M., McGimsey, R., Neal, C., 2013. Degassing of CO2, SO2, and H2S associated with the 2009 eruption of Redoubt Volcano, Alaska. Journal of Volcanology and Geothermal Research 259, 270–284.

Wohletz, K.H., Sheridan, M.F., Brown, W.K., 1989. Particle-size distributions and the sequential fragmentation transport-theory applied to volcanic ash. Journal of Geophysical Research 94, 15703–15721.